Investigation of hydroxyl radical recycling reactions in aldehydes
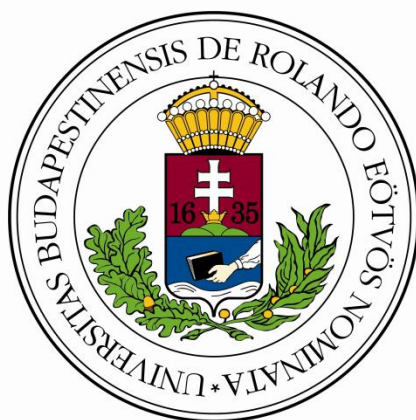
Thesis

Chemistry MSc

Tamás Varga

Supervisor: Prof Paul W. Seakins

Consultant: Prof Tamás Turányi

University of Leeds, School of Chemistry

Eötvös Loránd Tudományegyetem, Budapest

Természettudományi Kar

Kémia Intézet

Védés helye: Fizikai Kémia Tanszék

2013

Contents

3

Introduction

The hydroxyl radical is known to be one of the most important trace species in the atmosphere[1]. In most cases the hydroxyl radical initiates the oxidation process of hydrocarbons. A large amount of research has been aimed at understanding the chemistry of OH radicals in the atmosphere. Recent complex chemical models have been shown to adequately describe the concentration changes of OH in the atmosphere at non-complex conditions, showing that the understanding of the chemistry of OH is improving.[1]

An unusually large discrepancy was noticed between chemical modelling and measurements by several field campaigns in low NO_x, high biogenic VOC (volatile organic compound) environments. In highly forested areas a significant degree of under predicting OH levels was found by the PROPHET[2], AEROBIC97[3] and LBA-CLAIR·10-2001[4] projects. It was noted that the difference correlates with the measured isoprene levels, suggesting that isoprene and its decomposition products are linked to this effect. It was also noted that the main difference between the forested areas where this discrepancy arises and other places where models perform acceptably is the lack of anthropogenic NO_x.

It was apparent that either an OH source is not being accounted for or the amount of complex volatile hydrocarbons is underestimated. This spurred interest in the field and theoretical papers were published trying to identify a new reaction channel. A channel that recycles hydroxyl radicals during the atmospheric oxidation of isoprene was found by da Silva[5]. The reaction scheme consists of the addition of OH to one of the double bonds of isoprene and is followed by the addition of oxygen to the radical. This peroxy radical is capable of internally abstracting the hydrogen atom of the OH group. After this step the molecule undergoes prompt decomposition into OH and other oxygenated compounds.

A theoretical study have also been carried out by da Silva[6] on the same decomposition channel in methacrolein, one of the oxidation products of isoprene. The paper suggests that the exothermicity of the OH addition and subsequent O_2 addition could be enough for an internal hydrogen abstraction to take place, followed by decomposition into OH. Similar results were published on acrolein by Asatryan et al.[7].

Michael et al.[8] observed the formation of OH during the reaction of acetyl radicals with oxygen at low pressures. Later investigations found that this OH source is a very similar reaction channel to that which is occurring during isoprene oxidation. The differences are that

the initial reaction with OH abstracts a hydrogen atom as there is no carbon-carbon double bond and the internal hydrogen abstraction is from the carbon chain. The scheme is summed up in the following figure.
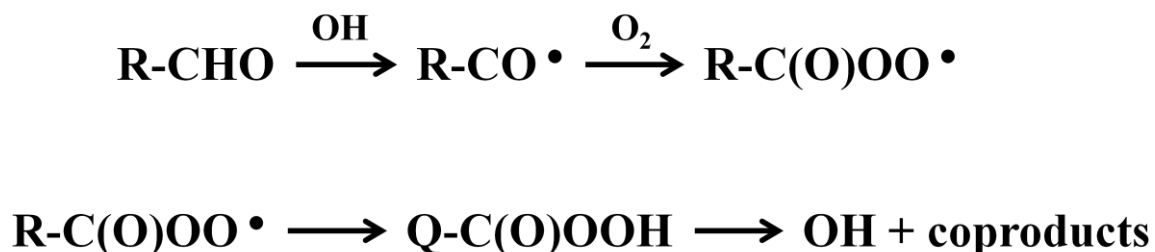
$$R\text{-}CHO \xrightarrow{\text{OH}} R\text{-}CO^{\bullet} \xrightarrow{\text{O}_2} R\text{-}C(O)OO^{\bullet}$$

$$R\text{-}C(O)OO^{\bullet} \longrightarrow Q\text{-}C(O)OOH \longrightarrow OH + coproducts$$

Figure 1. Reaction scheme of hydroxyl radical recycling in aldehydes.

For aldehydes thermal energy at room temperature is not enough for the internal hydrogen abstraction step. The exothermicity of the association reaction can provide enough excess energy for the decomposition channel. As the excess energy can also be lost by collisions with other molecules the yield of decomposition into OH is pressure dependent. The yield of this channel as a function of the pressure was investigated in several studies, but discrepancies still exist in the literature of this field.

During this research project the OH recycling reactions of aldehydes have been investigated using flash photolysis – LIF technique. My aim was to determine the yields of the decomposition of the alkoxy radicals in the presence of oxygen. C_2 through C_4 straight chained aldehydes have been investigated.

The same experiments have been performed on acrolein and methacrolein to determine if they are capable of hydroxyl radical recycling as suggested by da Silva[6] and Asatryan et al.[7].

Review of Selected Literature

In this section I describe the literature relevant to the decomposition reactions of peroxy radicals into hydroxyl radicals. First I discuss the experimental and theoretical results published on the OH recycling channel in aldehydes. This is followed by the summary of literature on OH recycling in the atmosphere and on papers that predict OH recycling to occur in the oxidation products of isoprene.

OH recycling in aldehydes

Several papers have been published on the OH recycling channel occurring in aldehydes. It was generally found, that the yield of the decomposition channel only becomes significant well below atmospheric pressures, at around 20 Torr. This means that these reactions are not responsible for significant contribution to atmospheric OH recycling. However this class of reactions are thought to play a role in low temperature ignition of hydrocarbons[9] and dimethyl-ether[10] as a chain propagation route. In the following sections I discuss the previously published experimental and theoretical results relevant to each aldehyde.

Acetaldehyde

Acetaldehyde is the most thoroughly investigated molecule among straight chained aldehydes. Its reaction with hydroxyl radicals and the subsequent recycling in presence of is generally accepted to follow the scheme described below. In the reaction with OH a hydrogen atom is abstracted from acetaldehyde. As the C-H bond of the α-carbon is significantly weaker than those of the beta carbon, the product is almost exclusively an acetyl radical.

$$CH_3CHO + OH \rightarrow CH_3CO \bullet + H_2O \qquad (R1)$$

In the presence of oxygen molecules, an addition reaction can occur to the radical site creating a peroxy radical.

$$CH_3CO \bullet + O_2 \rightarrow \left[CH_3C(O)OO\bullet\right]^* \qquad (R2)$$

The peroxy radical can have significant excess energy compared to the thermal energy when it is created, due to the exothermicity of the reaction (~140 kJ/mol[11]). This excited radical can lose its excess energy primarily via two channels. The peroxy radical group can abstract a hydrogen atom from the methyl group of the molecule forming a Q(O)OOH

6

radical. This step is followed by unimolecular decomposition into a lactone and a hydroxyl radical.

$$CH_3CO\bullet + O_2 \rightarrow [CH_3C(O)OO\bullet]^* \qquad (R3)$$

$$[CH_2\bullet C(O)OOH] \rightarrow cyc - CH_2C(O)O + OH \qquad (R4)$$
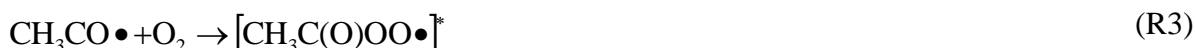
Other decomposition channels have been identified using theoretical methods[11], such as the decomposition of the Q(O)OOH radical into $CH_2=C=O$ and HO_2. However all these theoretically identified pathways exhibit energy barriers at least 12 kJ/mol higher than the OH channel, making them unfavoured at room temperature.

The other process is collisional relaxation, in which the peroxy radical collides with other molecules and transfers some of its energy to the collision partner. This way the acetyl radical can lose all its excess energy, and become thermalized. As the energy barrier of the internal hydrogen abstraction is much higher than the thermal energy at room temperature, the thermalized molecules are unable to follow the decomposition pathway.

$$[CH_3C(O)OO\bullet]^* \rightarrow [CH_3C(O)OO\bullet] \qquad (R5)$$

These $R(O)O_2$ radicals do not react further on the timescale of the reaction of aldehydes with OH. In an experiment where no further compounds are present they can be considered inert at room temperature. In the atmosphere they are depleted by converting NO to NO_2 and are further oxidized by oxygen.

Several papers have been published on the reaction of acetaldehyde with hydroxyl radicals. It was assumed in all publications that the main reaction channel is the abstraction of the hydrogen atom from the aldehyde group. These results are summarized in the following table.

Reference	Rate coefficient at 298 K / $cm^3 \, mol^{-1} \, s^{-1}$	Technique
	acetaldehyde + OH	
Zhu et al.[12]	$1.50 \cdot 10^{-11}$	Laser flash photolysis, LIF
Taylor et al.[13]	$1.50 \cdot 10^{-11}$	Flash photolysis, GC-MS
Wang et al.[14]	$1.67 \cdot 10^{-11}$	Laser flash photolysis, IR
Sivakumaran et al.[15]	$1.50 \cdot 10^{-11}$	Laser flash photolysis, LIF
D'Anna et al.[16]	$1.44 \cdot 10^{-11}$	Photolysis, FTIR
Scollard et al.[17]	$1.62 \cdot 10^{-11}$	Photolysis, GC
Balestra-Garcia et al.[18]	$1.69 \cdot 10^{-11}$	Flash photolysis, LIF
Dóbé et al.[19]	$1.71 \cdot 10^{-11}$	Electron beam, fluorescence
Semmes et al.[20]	$1.24 \cdot 10^{-11}$	Flash photolysis, LIF
Michael et al.[8]	$1.55 \cdot 10^{-11}$	Electron beam, fluorescence
Niki et al.[21]	$1.60 \cdot 10^{-11}$	Photolysis, FTIR
Atkinson et al.[22]	$1.62 \cdot 10^{-11}$	Flash photolysis, LIF
Morris el at.[23]	$1.50 \cdot 10^{-11}$	Electron beam, MS

Table 1. Summary of published rate coefficients for the reaction acetaldehyde + OH.

Almost results fall in the range of $1.5 - 1.7 \cdot 10^{-12} cm^3 molecule^{-1} s^{-1}$ with $1.63 \cdot 10^{-12} cm^3 molecule^{-1} s^{-1}$ being recommended by Baulch et al.[24] for room temperature. Due to the large number of measurements and small difference between results it can be considered a very well characterised reaction.

The rate constant for oxygen addition to the acetyl radical has been published at room temperature in several papers. They have obtained results for the rate coefficient in the range of $2.0 - 6.0 \cdot 10^{-12} cm^3 molecule^{-1} s^{-1}$, at room temperature for the high pressure limit rate constant of the reaction. The reported values can be found in the following table.

Reference	Rate coefficient at 298 K / $cm^3 \, mol^{-1} \, s^{-1}$	Technique
	acetyl + O2	
Kovács et al.[25]	$1.00 \cdot 10^{-12}$	Discharge flow, LIF
Tyndall et al.[26]	$5.70 \cdot 10^{-12}$	Flash photolysis, resonance fluorescence
Tyndall et al.[27]	$3.20 \cdot 10^{-12}$	Photolysis, FTIR
Sehested et al.[28]	$4.40 \cdot 10^{-12}$	Vis/UV absorption
McDade et al.[29]	$2.01 \cdot 10^{-12}$	Photolysis, MS
Romero et al.[30]	$5.07 \cdot 10^{-12}$	Laser flash photolysis, LIF

Table 2. Summary of published high pressure limit rate coefficients for the association reaction acetyl + O$_2$.

The first to observe OH production from the reaction of acetyl radicals with oxygen at low pressures were Michael et al.[8] but they did not quantify the effect. Tyndall et al.[27] quantified the OH yield as a function of pressure using a phenomenological model.

Later studies have investigated the decomposition channel of the acetyl-peroxy radicals. Blitz et al.[31] observed the OH production directly using LPF-LIF following the photolysis of acetone to acetyl and methyl radicals, and monitoring the OH produced by the acetyl + O_2 reaction. They have assigned relative yields to different pressures, and they obtained absolute OH yields by assuming a yield of unity at zero pressure. Carr et al.[32] used a similar method to photolyse acetic acid into acetyl radicals and OH. This provided an internal calibration for OH and absolute yields OH yields for the acetyl + O2 channel were obtained. These results were in good agreement with Blitz et al.[31], however yields were higher than those observed by Tyndall et al.[27].

Kovács et al.[25] investigated the acetaldehyde + OH reaction in a flow tube in the presence of oxygen. The reaction produce acetyl radicals which after reacting with oxygen can produce OH. The concentration of OH was measured and relative yields of the OH producing channel were obtained from the apparently decreased rate of OH decay due to recycling. The results showed agreement with the paper of Tyndall et al.[27]

Carr et al.[11] performed further measurements using photolysis of acetone as the source of acetyl radicals in helium and nitrogen bath gases. They also performed master equation simulations of the reaction system, based on a potential energy surface calculated at the G3X(MP2)-RAD level of theory, and found the simulation results to be consistent with their experiments.

The products of this reaction route were directly observed by Chen and Lee[33]. They have used step scan FTIR to analyze the products of the reaction. They have assigned the carbonyl stretch vibration mode at 1960 cm^{-1} to the α-lactone cyc-CH$_2$-C(O)O, proving that a lactone is produced during the decomposition of the peroxy radical. Romero et al.[34] and Devolder et al.[35] observed production of HCHO at longer timescales suggesting fragmentation of the lactone into HCHO + CO.
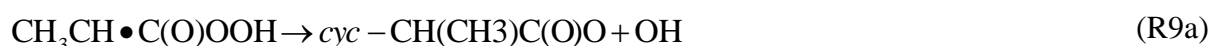
Propionaldehyde

The reaction of propionaldehyde and hydroxyl radicals follows essentially the same scheme as acetaldehyde. The hydrogen abstraction by hydroxyl radicals primarily occurs from the alpha hydrogen. If oxygen is present it can add to the

$$CH_3CH_2CHO + OH \rightarrow CH_3CH_2CO \bullet + H_2O \tag{R6}$$

$$CH_3CH_2CO \bullet + O_2 \rightarrow CH_3CH_2C(O)O_2 \bullet \tag{R7}$$

The peroxy radical has two different sites to abstract a hydrogen atom from, the beta and gamma carbons.

$$CH_3CH_2C(O)O_2 \bullet \rightarrow CH_3CH \bullet C(O)OOH \tag{R8a}$$

$$CH_3CH_2C(O)O_2 \bullet \rightarrow CH_2 \bullet CH_2C(O)OOH \tag{R8b}$$

This is followed by decomposition into OH and an alpha or beta lactone respectively.

$$CH_3CH \bullet C(O)OOH \rightarrow cyc - CH(CH3)C(O)O + OH \tag{R9a}$$

$$CH_2 \bullet CH_2C(O)OOH \rightarrow cyc - CH_2CH_2C(O)O + OH \tag{R9b}$$

The stabilization of the peroxy radicals increases with the carbon chain length, favouring relaxation instead of the decomposition channel compared to the acetyl-peroxy radicals. In case of the formation of β-Q(O)OOH radicals a similar energy barrier is expected to acetyl-peroxy radicals. The γ-Q(O)OOH radical formation however is expected to have a lower barrier, as the transition state requires a six atom ring to form which is a less rigid structure than the five atom rings required for the β-Q(O)OOH formation or in the case acetaldehyde.

The β-Q(O)OOH radical is a tertiary radical which makes it more stable than the γ-Q(O)OOH, as higher order radicals are generally more stable than the lower order radicals with identical functional groups and carbon chain lengths. Due to this increased stability the possibility of collisional relaxation of Q(O)OOH radicals as well as the $R(O)O_2$ radicals also arises, which could decrease OH yields.

The reaction of propionaldehyde with hydroxyl radicals has been extensively investigated. It was generally assumed that primary route is the abstraction of the α-hydrogen. The published rate coefficients can be seen in the following table.

Reference	Rate coefficient at 298 K / $cm^3\,mol^{-1}\,s^{-1}$	Technique
propionaldehyde + OH		
Le Crane et al.[36]	$1.86 \cdot 10^{-11}$	Photolysis, FTIR
Baker et al.[37]	$1.70 \cdot 10^{-11}$	Photolysis, GC
D'Anna et al.[16]	$1.90 \cdot 10^{-11}$	Photolysis, FTIR
Thevenet et al.[38]	$2.06 \cdot 10^{-11}$	Laser flash photolysis, LIF
Papagni et al.[39]	$2.02 \cdot 10^{-11}$	Photolysis, GC
Semmes et al.[20]	$1.71 \cdot 10^{-11}$	Flash photolysis, resonance fluorescence
Kerr et al.[40]	$1.79 \cdot 10^{-11}$	Photolysis, GC
Audley et al.[41]	$1.78 \cdot 10^{-11}$	Photolysis, GC
Niki et al[21]	$2.09 \cdot 10^{-11}$	Photolysis, FTIR

Table 3. Summary of published rate coefficients for the reaction propionaldehyde + O_2.

Only one value for the association reaction of the propionyl radical with oxygen has been published, by Romero et al.[30] They reported a high pressure limit rate constant of $5.37 \cdot 10^{-12}$ $cm^3\,mol^{-1}\,s^{-1}$ which suggests a similar rate as in the case of the reaction of acetyl radicals with oxygen.

Two experimental papers have been published concerning OH yields from the reaction of propionyl radicals with oxygen. Romero et al.[30] measured the OH yields from this reaction using PLF-LIF method, in helium bath gas in the pressure range of $10 - 400$ Torr at temperatures 298K and 212 K. Similar experiments were carried out by Zügner et al. [42] using low pressure discharge flow technique coupled with resonance fluorescence monitoring of OH radicals. They have obtained significantly lower yields from their experiments compared to those of Romero et al. The authors attempted to use theoretical results coupled with master equation modelling to determine which set of results is correct, but they have not been able to obtain a conclusive answer.

Butyraldehyde

In the case of butyraldehyde no studies have been published that investigate hydroxyl radical recycling channels. The same general reaction scheme is expected to take place, with further sites from which the internal hydrogen abstraction can occur.

In the literature rate coefficients for the reaction of butyraldehyde with hydroxyl radicals have been published, but none for the association reaction of butyryl radicals with oxygen or the hydroxyl radical yield of the association reaction. The published results can be seen in the following tables.

Reference	Rate coefficient at 298 K / $cm^3 mol^{-1} s^{-1}$	Technique
butyraldehyde + OH		
Albaladejo et al.	$2.88 \cdot 10^{-11}$	Laser flash photolysis, LIF
D'Anna et al.[16]	$2.38 \cdot 10^{-11}$	Photolysis, FTIR
Papagni et al.[39]	$2.47 \cdot 10^{-11}$	Photolysis, GC
Semmes et al.[20]	$2.27 \cdot 10^{-11}$	Flash photolysis, resonance fluorescence
Kerr et al.[40]	$2.41 \cdot 10^{-11}$	Photolysis, GC
Audley et al.[41]	$2.52 \cdot 10^{-11}$	Photolysis, GC

Table 4. Summary of published rate coefficients for the reaction butyraldehyde + O_2.

OH recycling reactions in the atmosphere

The need to investigate channels of OH recycling in atmospheric oxidation reactions originates from the findings of several field measurements. It was found by several field campaigns, such as the PROPHET[2], AEROBIC97[3] and LBA-CLAIR·10-2001[4] projects that the concentration of OH is severely under predicted by current models in certain regions. Interestingly, the OH concentrations measured in the atmospheric boundary layer are in good agreement with modelling results, which suggested that the source of discrepancy are a set of conditions that have been failed to be taken into account in our models.

It was found that the difference between measurements and models can be linked to high volatile organic compound emissions in areas with NO_x levels. This corresponds to highly forested areas, where the plants are the source of VOCs but there is no anthropogenic NO_x to participate in the oxidation process.

The general oxidation scheme for VOCs was thought to be well understood. The first step is H abstraction from the carbon chain by OH or the addition of the hydroxyl radical to one of the double bonds. An organic radical is formed which then forms an alkylperoxy radical in an association reaction with oxygen. These radicals react with NO to produce NO_2 and HO_2 to form various oxygenated products. The same route is followed by these products until CO/CO_2 and water is produced. These processes can be summed up in the following scheme.
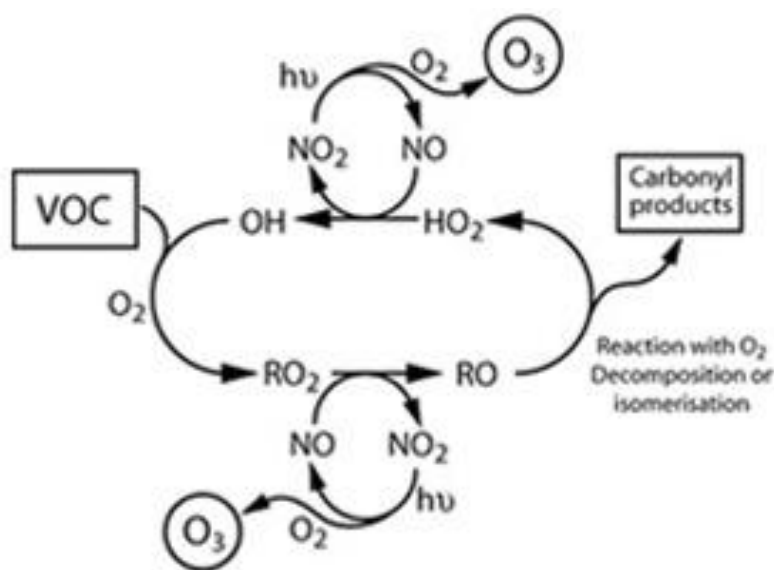

Figure 2. General reaction scheme of atmospheric oxidization of VOCs. Figure adapted from Clapp et al.[43], by the Manchester Centre for Atmospheric Science[44].

This means that it would be expected, that a large concentration of VOCs depletes the atmospheric OH concentrations. Considering the previously mentioned experimental results it became obvious that an important class of reactions is unknown that offers an oxidation route without OH consumption.

Theoretical studies were conducted on the VOCs that are primarily emitted in forested areas such as isoprene. It was found by da Silva[5], that during the oxidation of isoprene some of the alkylperoxy radicals are capable of unimolecular decomposition into OH and other oxygenated compounds such as methacrolein, methyl vinyl ketone, and formaldehyde. The reaction mechanism involves the addition of an OH radical to one of the primary carbon atoms of isoprene, which is followed by the addition of oxygen to the adjacent carbon atom. Then an internal hydrogen abstraction can occur from the hydroxyl group to the peroxy group. This step has an unusually low barrier and leads to the prompt, barrierless decomposition into OH and other oxygenated products. The energy diagram calculated by da Silva can be seen in the following figure.
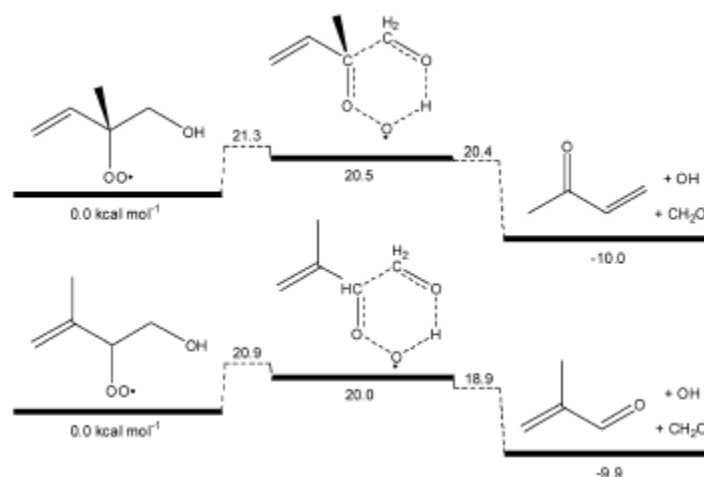

Figure 3. Energy diagrams for the OH recycling channels occurring during the oxidation of isoprene. Energies were calculated using the average results of the G3SX and CBS-QB3 method at 298 K, and are given in kcal mol^{-1} units. Figure was taken from the paper of da Silva.[5]

It was found that the barrier of the hydrogen abstraction from the hydroxyl group a height of 21.3 and 20.9 kcal mol^{-1}, for the tertiary and secondary peroxy radical groups respectively. This is unusually low for hydrocarbons, and makes the OH recycling channels possible. Applying TST theory to the results and taking tunnelling effects into consideration

with a one dimensional Eckart potential, a unimolecular rate was obtained for this reaction channel. The result is a rate coefficient of around $10^{-3} – 10^{-4}\, s^{-1}$ at 300 K. This means that the alkylperoxy radicals must have a lifetime of around 100-1000 seconds for the unimolecular decomposition channel to be significant. This could only occur in clean NO_x free regions, which explains why the effect was not present in polluted areas where there is also a large emission of VOCs.

In later studies da Silva[6] and Asatryan et al.[7] investigated whether some the products of isoprene oxidation, could exhibit similar reaction channels. Using theoretical chemical methods da Silva found that the peroxy radicals formed form methacrolein might be capable of unimolecular decomposition into OH. It was found that the energy barrier for the internal hydrogen abstraction is higher than in the case of isoprene and would be too high to pass if the only excess energy originates from the O_2 addition. He concluded that for OH recycling to occur, the peroxy radicals would have to retain some of their excess energy from the hydrogen abstraction step by OH, when obtaining further energy from the oxygen addition.   Asatryan et al.[7] found similar results for acrolein, the homologue of methacrolein.

I have found no published papers on the investigation of the hydroxyl radical recycling channel in either acrolein of methacrolein. There are some results available for their reaction with hydroxyl radicals. The published results are summed up in the following tables.

Reference	Rate coefficient at 298 K / $cm^3 \, mol^{-1} \, s^{-1}$	Technique
acrolein + OH		
Orlando et al.[45]	$2.00 \cdot 10^{-11}$	Photolysis, FTIR
Magneron et al.[46]	$2.00 \cdot 10^{-11}$	Laser flash photolysis, LIF
Edney et al.[47]	$2.04 \cdot 10^{-11}$	Photolysis, GC
Atkinson et al.[48]	$1.83 \cdot 10^{-11}$	Photolysis, GC
Kerr et al.[40]	$1.91 \cdot 10^{-11}$	Photolysis, GC

Table 5. Summary of published rate coefficients for the reaction acrolein + O_2.

References	Rate coefficient at 298 K / $cm^3 \, mol^{-1} \, s^{-1}$	Technique
methacrolein + OH		
Chuong et al.[49]	$3.22 \cdot 10^{-11}$	Discharge flow resonance fluorescence
Chuong et al.[50]	$3.23 \cdot 10^{-11}$	Discharge flow, resonance fluorescence and Discharge flow , LIF
Orlando et al.[45]	$2.80 \cdot 10^{-11}$	Photolysis, FTIR
Gierczak et al.[51]	$2.76 \cdot 10^{-11}$	Laser flash photolysis, LIF
Edney et al.[47]	$3.92 \cdot 10^{-11}$	Photolysis, GC
Atkinson et al.[48]	$2.86 \cdot 10^{-11}$	Photolysis, GC
Kleindienst et al.[52]	$3.20 \cdot 10^{-11}$	Flash photolysis, Resonance fluorescence

Table 6. Summary of published rate coefficients for the reaction methacrolein + O_2.

Description of the experimental apparatus

In this section, first I describe the Laser Flash Photolysis – Laser Induced Fluorescence technique. Then I describe the experimental apparatus that I used to conduct the experiments, and finally briefly describe the methods used for the master equation simulations of the reaction systems.

Laser flash photolysis

Many atmospherically relevant reactions take place between a closed shell molecule and an open shell radical. This makes the investigation of such reactions difficult as most radical species are extremely reactive therefore cannot be prepared in advance of an experiment. Radicals generally have to be produced in situ if we wish to study their reactions. This is usually done by utilizing chemical or photochemical reactions.

For reaction kinetic studies it is important that the rate of production of radicals is much faster than the rate of the reaction that is to be studied, so that the two processes can be handled independently. Using a chemical reaction as the source of a radical can be difficult for several reasons. Generally two or more precursor molecules are required which introduces the risk of the precursors interfering with the studied reaction. The rate of production of radicals is limited by the concentration of the precursors. Increasing the amount of precursors can be used to shorten the timescale of radical formation, but this can increase the interference from secondary reactions. These difficulties limit the applicability of chemical reactions as a radical source in kinetic studies.

Photolysis is usually a more convenient method for producing radicals than chemical reactions. A suitable precursor molecule is needed which can undergo decomposition into the required radical molecule when excited by light of an appropriate wavelength. Photochemical reactions are practically instantaneous which is ideal for kinetic studies. If a short flash is used to photolyse the precursor compound, the starting point of the reaction is well defined. However the duration of irradiation has to be significantly shorter than the characteristic timescale of the studied reaction to separate the two processes.

Pulsed lasers are ideal light sources for photolysis. A pulse width of a few nanoseconds can be achieved for excimer lasers or by using Q-switching in solid state lasers, which is generally a short enough duration to study any bimolecular reaction. Lasers are also

monochromatic which makes selective excitation of the radical precursor compounds possible.

Laser induced fluorescence method

Laser induced fluorescence is a spectroscopic technique, that can be used for the detection of molecular species. It is required of the molecule to have one or more electronically excited state which relaxes through fluorescence with a high yield, at the conditions where its concentration is to be measured. The basis of the method is to excite the molecules with a laser that has a wavelength that corresponds at an electronic absorption band of the molecule. Then the fluorescent light emitted by the excited molecules as they relax to their electronic ground state is collected and detected using a photomultiplier tube (PMT). The signal from the fluorescence is directly proportional to the amount of the excited molecules. Therefore it is also proportional to the amount of the molecules.

When a molecule absorbs a photon of the laser it is excited to one of its electronic excited states and is usually also vibrationally excited. In most cases the excited molecule undergoes vibration relaxation, and reaches the vibrational ground state before returning to its ground state via fluorescence. Also, during fluorescence the molecule does not necessarily return to the vibrational ground state. The reason for this effect is that the Frank-Condon factors of the electronic-vibronic transitions favour those transitions in which the equilibrium atomic separations are most similar. This usually corresponds to a vibrational excited state when moving from a vibrational ground state.

Therefore some energy is lost due to relaxation, between the exciting photons and the emitted photons. A typical laser induced fluorescence excitation and collection scheme can be seen in the following figure.
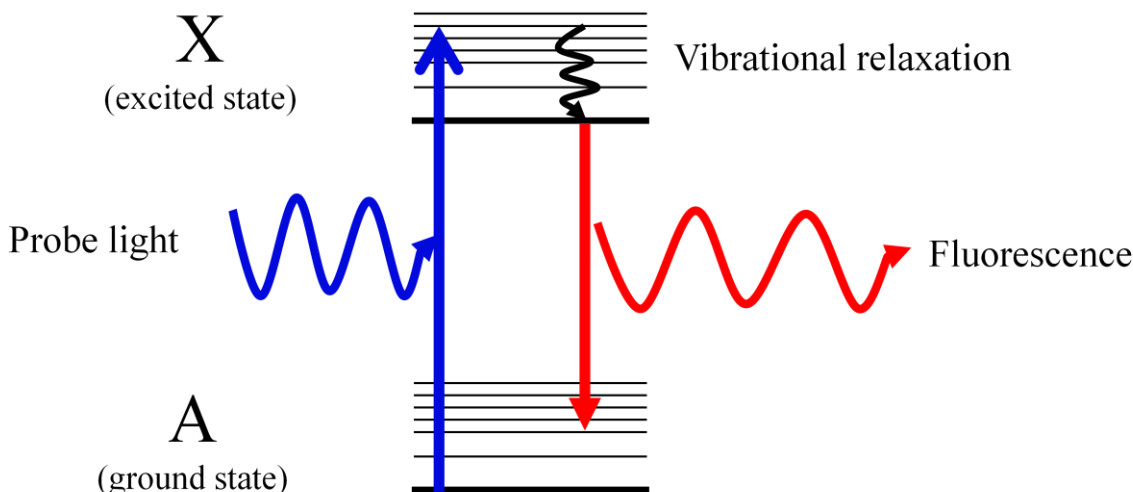
Figure 4. Typical excitation and fluorescence collection scheme. The molecules in electronic and vibrational ground state are excited both electronically and vibrationally by the probe laser. The excited molecules first reach the vibrational ground state of the electronically excited state, then return to one of the vibrational states of the electronic ground state. The emitted light is of longer wavelength than the probe laser.

In such cases by applying a filter with an appropriate cut-off band before the detector the probe light can be filtered and will not interfere with the detection. However if the difference between the absorption and emission wavelengths too small, the filter cannot perfectly block out the probe light. In these cases the scattered light can still be separated from the fluorescence if is ha a shorter duration than the fluorescence lifetime. The different time scales of scattering and fluorescence can be used to identify the signal that originates from the probe laser, and can be cut off using an appropriate gating function.

The electronically excited molecules can also return to their ground state by collisional quenching. In such events an excited molecule collides with another different molecule and passes its excess energy to its collision partner, without emitting light. The efficiency of quenching depends on the collision partner. In gas phase this can be considered the only competing process to fluorescence, therefore the fluorescence yield can be written in the following form.

$$\Phi_{fluor} = \frac{k_{fluor}}{k_{fluor} + \sum_{i=1}^{N} k_{quench,i}[Q_i]} \tag{1}$$

In the equation k_{fluor} is the rate of relaxation via fluorescence and $k_{quench,i}$ is the second order quenching rate coefficient for component Q_i. It can be seen, that the higher the concentration of quenching molecules is, the lower the yield of fluorescence will be. This means that at higher pressures the method is less sensitive as less fluorescence photons are emitted.

Quenching also shortens the lifetime of the excited state, therefore the fluorescence lifetime is also reduced. The change in lifetime can be described by the following equation.

$$\frac{1}{\tau_{exc}} = \frac{1}{\tau_{flour}} + \frac{1}{\tau_{quench}} \tag{2}$$

The quenching characteristic time can be obtained by the following equation.

$$\tau_{quench} = \frac{1}{\sum_{i=1}^{N} k_{quench,i}[Q_i]} \tag{3}$$

At high enough concentration of quenching agents the fluorescence signal cannot be differentiated from the scattered light due to its short lifetime. This can make measurements difficult or impossible at higher pressures if the bath gas can quench fluorescence, as it is in the case of nitrogen.

Determining rate coefficients based on LIF

The LIF method can be used for detecting species during kinetics experiments. If the concentration of one of the reactants in a reaction can be measured as a function of the time, a rate constant can be obtained for the reaction. During this research project laser induced fluorescence was used to monitor hydroxyl radicals, I will only discuss applications for this molecule.

Using the LIF method absolute concentrations cannot be obtained without calibration. In reaction kinetic experiments if the decay of a molecule is first order, its relative concentration alone is enough to determine the rate coefficient of the decay and determination of absolute concentrations is unnecessary.

Consider the reaction of a molecule with OH. The rate of change in the concentration of OH, in homogeneous conditions can be described in the following way.

$$\frac{d[OH]}{dt} = -k[OH][reactant]$$

(4)

If the concentration of the reactant is in large excess compared to the concentration of OH, the concentration of the reactant does not change due to reaction taking place. This means that the product of the rate coefficient and the concentration of the reactant can be reduced into one term.

$$k' = k[reactant]$$

(5)

$$\frac{d[OH]}{dt} = -k'[OH]$$

(6)

k' is called the pseudo-first order rate coefficient. Integrating the equation we get the following relation between the time since the start of the reaction and the relative OH concentration.

$$[OH](t) = [OH]_0 \exp(-kt)$$

(7)

$$\frac{[OH]}{[OH]_0}(t) = \exp(-kt)$$

(8)

Varying the delay between the start of the reaction and the firing of the probe laser, the relative concentration of OH can be obtained as a function of reaction time. An exponential decay model can be fitted to the relative concentration − time data points, which can be used to determine the pseudo first order rate coefficient.

To determine the second order rate coefficient of the reactant + OH reaction, several experiments have to be conducted, at different reactant concentrations while keeping all other conditions constant. The second order rate constant can be obtained by a linear fit of the pseudo-first order rate coefficients as a function of the reactant concentration. The second order rate constant is the slope of the fitted line. The standard deviations of the pseudo-first order rate coefficients were available from their respective fits, so they were used as weights during the fitting of the second order rate coefficient. An example can be seen in figure the following figure.
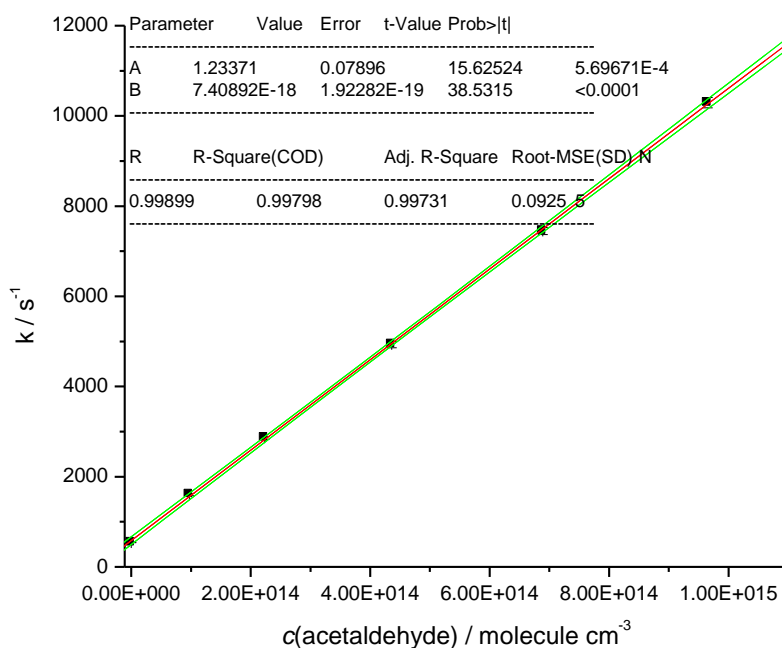
Figure 5. Measured apparent first order rate constants of the acetaldehyde + OH reaction, as the function of the acetaldehyde concentration. The black squares show the measured values, the red continuous line the fit and green continuous lines the confidence intervals of the fit. The second order rate constant is $7.41 \cdot 10^{-18}$ cm^3 mol^{-1} s^{-1}. Conditions are $p = 10$ Torr, $T = 298$ K, 10% oxygen, 90 % nitrogen.

Determination and interpretation of OH yields

To measure the ratio of OH recycling, the rate coefficient of the reaction between acetaldehyde and OH radicals has to be measured in absence of oxygen. This is the rate coefficient of the H abstraction. Then the rate has to be measured in presence of oxygen at the same conditions. The apparent rate will be slower, since some of the OH that reacted with the aldehyde will be recycled.

The OH yield is equal to the ratio of the decrease of the apparent rate coefficient in the presence of oxygen, compared to the rate coefficient that can be measured in its absence.

This can be expressed by the following equation.

$$\Phi_{OH} = \frac{k_{nitrogen} - k_{oxygen}}{k_{nitrogen}} \qquad (9)$$

This can be simplified to the following form.

$$\Phi_{OH} = 1 - \frac{k_{oxygen}}{k_{nitrogen}} \tag{10}$$

The following figure demonstrates measured pseudo-first order rate coefficients and the fitted second order rate coefficients in both with nitrogen and oxygen bath gas at different pressures.
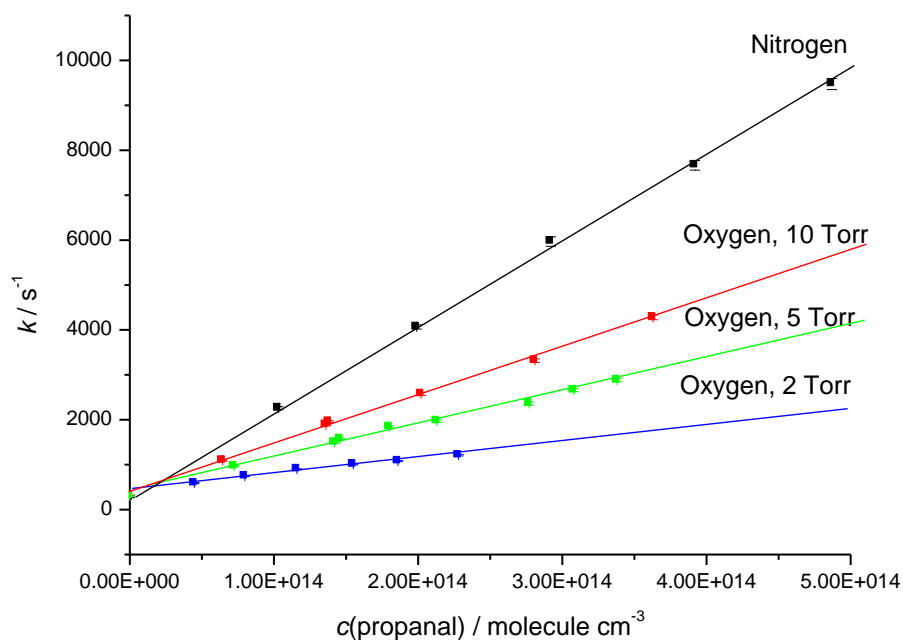
Figure 6. Plot of pseudo first order rate coefficients and the fitted second order rate coefficients for the propionaldehyde + OH reaction. Results obtained with nitrogen bath gas are plotted with black points and continuous line. Results obtained in oxygen are plotted with coloured points and continuous lines.

The OH yield is pressure dependent as it is determined by the ratio of the rates of unimolecular decomposition of the peroxy radicals and the rate of their collisional deactivation. This can be expressed by the following equation.

$$\Phi_{OH} = \frac{k_{OH}}{k_{OH} + k_Q [\text{M}]} \tag{11}$$

23

If we take the inverse of equation (11), we get the following expression.

$$\frac{1}{\Phi_{OH}} = \frac{k_{OH} + k_Q[\text{M}]}{k_{OH}} \tag{12}$$

$$\frac{1}{\Phi_{OH}} = 1 + [\text{M}]\frac{k_Q}{k_{OH}} \tag{13}$$

It can be seen that if we plot the inverse of the OH yield against the total concentration we should get a straight line. The intercept is expected to be one and the slope to be the ratio of the quenching rate coefficient and the rate of the decomposition channel that produces OH.

Experimental method

Description of the reaction cell

The cell used in our experiments is stainless steel 6-way cross reactor, fitted with quartz windows on each side. The excimer and probe laser light are let into the cell through two horizontal windows, perpendicularly to each other. The photomultiplier tube was set at the top of the cell so that the collection of fluorescence is perpendicular to both lasers.

A photodiode was also used, to measure the intensity of the probe laser. The measured signal is proportional to the number of excited OH molecules, which depends on the intensity of the probe laser. The intensity was also stored along with the measured fluorescence intensities and were used to normalize the values during data processing.

The temperature of cell was measured using a K-type thermocouple. The reaction cell was welded into a metal bath such that just the end flanges of the cell arms protrude through the walls of the bath. This way the bath could be filled with liquid to act as thermostat if temperatures different from room temperature were needed for the experiments. Measurements at 212 K were also performed apart from room temperature experiments. This temperature was achieved by using a chloroform – dry ice bath.

Description of the gas system

The LPF-LIF experiments require several reactant and diluting gases to be present in the reaction cell. The pressure in the cell has to be monitored and the exact compositions of the reaction mixture must be known.

The experiments required an OH precursor, the investigated molecule as reactant, nitrogen and oxygen as diluting gases. *Tert*-butyl peroxide was used as the hydroxyl radical precursor. *Tert*-butyl-peroxide can be photolysed to stoichiometrically produce OH.

$$t\text{-}C_4H_9OOH + h\nu \rightarrow OH + co\text{-}products \tag{R10}$$

The *tert*-Butyl-peroxide and reactant aldehydes were prepared in bulbs on a vacuum line. The bulbs were pumped down using a diffusion pump to ensure that they were free of oxygen before filling with the gas. Filling was done by preparing a pure liquid sample of the compound, which was also purged of oxygen and putting the sample onto the same evacuated line as the bulb. This way the bulb was filled up to the vapour pressure of the compound. The pressure inside the bulb was always measured and noted. The bulbs were filled with pure nitrogen up to about 1.3 atmosphere pressure. The mole fraction of the precursor and reactants could be calculated as the ratio of their partial pressures in the bulb assuming them to behave ideally.

The pure oxygen and nitrogen diluting gases were taken from gas cylinders and flown into the reaction cell.

The flow from the bulbs and gas cylinders into the reaction cell were controlled by mass flow controllers. The mass flow controllers were previously calibrated using bubble velocity method. A small number of flow measurements were carried out to validate the previous calibrations and all of them were found to be valid.

The reaction cell was continuously pumped by a rotary pump, and the pressure was monitored using a capacitance manometer. The exact pressure could be set by throttling the valve of the rotary pump. Overnight the cell was also pumped by a diffusion pump to remove all traces of the gases used during the measurements from the cell.

Description of the laser system

An off resonance fluorescence collection scheme was used for the detection of hydroxyl radicals after excitation. The $A^2\Sigma(v=1) \leftarrow X^2\Pi(v=0)$, $Q_1(1)$ transition OH was utilized with the probe laser light at 282 nm wavelength. The light was produced by a pulsed dye laser (Spectra Physics PDL-3) using Rhodamine6G dye. The dye laser was pumped by the 1064 nm output of a Nd:YAG laser (Spectra Physics GCR-150), frequency tripled to 355 nm.

25

The fluorescence was detected at 308 nm wavelength. To decrease interference from other light sources an interference filter (Corion, 310 ± 10 nm) was fitted before the window in front of the PMT.

Tert-Butyl peroxide was photolysed using a Lambda Physik Compex KrF excimer laser at 248 nm. The pulse from the excimer laser acts as the starting time of an experiment and the delay in the firing of the probe laser is relative to this. This way the starting time of the reaction and the time of measurement of the hydroxyl radicals is well defined.

The lasers were operated at 10 Hz pulse frequency to ensure that the reaction mixture in the cell is always refreshed. The typical probe laser output was 10-20 mJ/pulse, using a 285-288 ns Q-switch delay for the pumping Nd:YAG laser. Photolysis energies were typically 70-130 mJ/pulse.

Recording concentration profiles

In each experiment the aim is to determine the rate coefficient of the decay of the hydroxyl radicals. The relative concentration – time profile of the hydroxyl radicals has to be measured. This is done by varying the delay between the firing of the excimer laser that produces the OH radicals, and the probe laser that excites the OH radicals. The time interval in which the delay was changed was always modified according to the time scale of the current reaction rate. The typical timescales were around 1 ms when the highest concentrations of the reactant were used, and 25 ms in cases where no reactant molecule was flown into the cell.

The fluorescence light from the excited OH molecules was detected using a photomultiplier tube. To reduce the noise of the signal the initial scatted light detected by the PMT was processed using a boxcar averaging circuit. The width of the boxcar function was set manually at each different pressure, as the lifetime of the fluorescence signal is pressure dependent.

At higher pressures, approximately from 20 Torr, due to collisional quenching the lifetime of fluorescence was not long enough to be well separated from the scattered probe light. In these cases the gating could not separate the two sources of signal and the scattered light was also detected. This resulted in a significantly higher baseline and a lower signal to noise ratio but experiments could still be carried out with satisfactory precision.

Data processing

During the experiments the intensity of the fluorescence and the intensity of the probe laser light are recorded as a function of time, using a PMT and photodiode respectively. In each experiment a background signal also is recoded for both the PMT and photodiode. In case of the photodiode it is the signal that is recorded without the probe laser firing. In case of the PMT it is the signal that is recorded when the probe laser is firing but the excimer laser is not, so the baseline incorporates the signal from the scattered light.

The baselines are subtracted from the respective signals, and the measured signal is normalized, using the signal of the laser intensity. This way we obtain a signal-to-power ratio, which is then fitted with an exponential decal model. The equation we use is the following.

$$y = A_0 \cdot \exp(-t \cdot k) + y_0$$

y is the signal-to-power ratio, t is the delay between the excimer and probe laser pulses, A_0 is the signal-to-power ratio at zero time, and k is the apparent first order rate constant. Since the baselines are subtracted, the signal-to-power ratio should exponentially decrease to zero, but we found that a nonzero signal usually remains even a long timescales. This is probably due to the photolysis of peroxy radicals caused by the probe laser, and has to be taken into account with the y_0 parameter.

For the data processing and parameter fitting a simple program was created using the MINFIT C library. An example of an exponential decay and fit can be seen in the following figure.
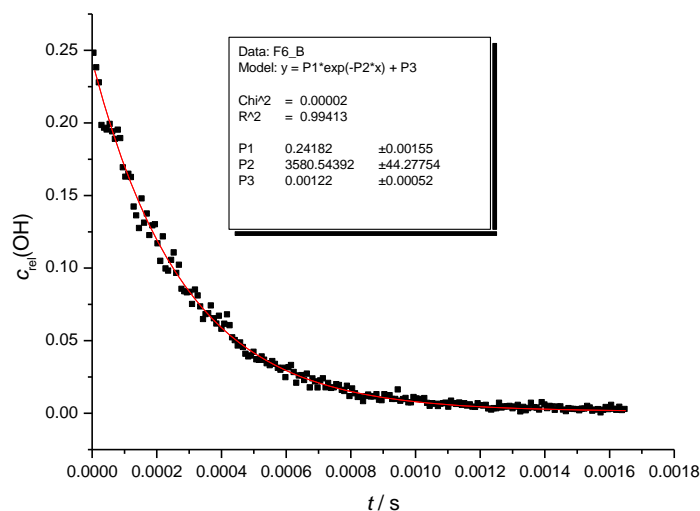
Data: F6_B
Model: y = P1*exp(-P2*x) + P3

Chi^2   = 0.00002
R^2   = 0.99413

P1   0.24182   ±0.00155
P2   3580.54392   ±44.27754
P3   0.00122   ±0.00052

Figure 7. Measured OH decay signal during reaction with acetaldehyde and fitted curve. Conditions are T = 298 K, p = 8.44 Torr, c(acetaldehyde) = $1.75 \cdot 10^{14}$ molecule cm^{-3}. The fitted rate constant is 3580 s^{-1}.

Master equation simulations

Master equation simulations were used to interpret the some of the data obtained in the experiments. The basic form of the problem to be solved is the following.

$$\frac{\mathbf{dp}}{\mathbf{d}t} = \mathbf{Mp}$$

Where **p** is a vector, of the populations of each state in the system, and **M** is matrix containing the rates of transition between each pair of states. For each molecular species the state space was divided into grains, and the density of states was obtained from rotational and vibrational constants calculated using theoretical chemical methods.

By performing these simulations the time evolution of the reaction system is obtained with respect to the populations of the different species and their energy distributions. The relative yields of the different possible reaction channels can be investigated in more direct way that a simple one step relaxation model.

The transitions that can occur in the system, described by the **M** matrix, are of two types. The first type is collisional energy transfer in which the internal energy of a molecule changes due to collisions, but it remains as the same species. The second type are chemical reactions.

28

Transition rates for collisional energy transfer are described by an exponential down model, parameterized with Lennard-Jones parameters obtained from the electronic structure calculations. The $<\Delta E>_{\text{down}}$ parameter was selected individually for each reaction system and also fitted to the measured data when possible.

The reaction rates as a function of internal energy were calculated using RRKM theory for isomerisation reactions. In case of association reactions of radicals with oxygen molecules this method cannot be employed due to the lack of a well defined reaction coordinate.

In these cases the sum of states of the transition state was obtained using inverse Laplace transformation. The following equation can be used to obtain the sum of states as a function of energy, for the transition state.

$$W(E) = hL^{-1}\left\{k_{\infty}(T)K_{eq}(T)Q_{R\bullet}(T)Q_{O_2}(T)\right\}$$

In the equation $L^{-1}\{\ \}$ is the inverse Laplace transformation operator, k_{∞} is the high-pressure association rate coefficient, K_{eq} is the equilibrium constant for the reaction and Q is the partition function of the given molecular species.

The high-pressure association rate coefficient has to be expressed as a function of the temperature. For this an extended Arrhenius type expression is used.

$$k_{\infty}(T) = A\left(\frac{T}{T_0}\right)^n \exp\left(\frac{-E}{kT}\right)$$

The equilibrium constant can be expressed both as the quotient of the association and dissociation rate constants and the quotient of the partition function of the reactants and products.

$$K_{eq}(T) = \frac{k_{\infty,-}(T)}{k_{\infty,+}(T)} = \frac{Q_{ROO\bullet}(T)}{Q_{R\bullet}(T)Q_{O_2}(T)}$$

The partition functions were obtained from the electronic structure calculations, while the Arrhenius parameters were selected based on direct experimental data.

Simulations were performed using the open-source MESMER program[53].

Results and discussion

In this section I describe and discuss the experimental results. The results obtained for each compound are discussed separately.

Acetaldehyde

A series of experiments were performed investigating the acetaldehyde + OH reaction, to determine the yield of the decomposition channel into OH in presence of oxygen. The experiments were conducted at room temperature (298 K) and in the pressure range of 1-20 Torr. The following table contains the summary of the second order rate coefficients measured during these experiments. The pressure values given in Torr-s are the nominal pressures that were approximately set for each experimental set. The M_{tot} values are the exact pressure values given in molecule cm^{-3} units.

Nitrogen				Oxygen			
p/ Torr	M_{tot} / cm^{-3}	k /cm^3 mol^{-1} s^{-1}	$\sigma(k)$	p/ Torr	M_{tot} / cm^{-3}	k / cm^3 mol^{-1} s^{-1}	$\sigma(k)$
				1	$3.343 \cdot 10^{16}$	$4.100 \cdot 10^{-12}$	$2.013 \cdot 10^{-13}$
1	$3.272 \cdot 10^{16}$	$1.332 \cdot 10^{-11}$	$1.552 \cdot 10^{-13}$	1	$3.415 \cdot 10^{16}$	$3.683 \cdot 10^{-12}$	$3.434 \cdot 10^{-14}$
2.5	$8.181 \cdot 10^{16}$	$1.297 \cdot 10^{-11}$	$6.414 \cdot 10^{-14}$	2.5	$7.920 \cdot 10^{16}$	$5.646 \cdot 10^{-12}$	$5.636 \cdot 10^{-14}$
3.5	$1.145 \cdot 10^{17}$	$1.314 \cdot 10^{-11}$	$1.041 \cdot 10^{-13}$	3.5	$1.100 \cdot 10^{17}$	$7.171 \cdot 10^{-12}$	$1.466 \cdot 10^{-13}$
5	$1.636 \cdot 10^{17}$	$1.318 \cdot 10^{-11}$	$5.767 \cdot 10^{-14}$	5	$1.605 \cdot 10^{17}$	$7.945 \cdot 10^{-12}$	$1.246 \cdot 10^{-13}$
10	$3.272 \cdot 10^{17}$	$1.378 \cdot 10^{-11}$	$1.729 \cdot 10^{-13}$	10	$3.422 \cdot 10^{17}$	$1.003 \cdot 10^{-11}$	$5.891 \cdot 10^{-14}$
15	$4.909 \cdot 10^{17}$	$1.378 \cdot 10^{-11}$	$8.722 \cdot 10^{-14}$	15	$5.024 \cdot 10^{17}$	$1.104 \cdot 10^{-11}$	$1.405 \cdot 10^{-13}$
20	$6.545 \cdot 10^{17}$	$1.355 \cdot 10^{-11}$	$1.064 \cdot 10^{-13}$	20	$6.683 \cdot 10^{17}$	$1.172 \cdot 10^{-11}$	$2.871 \cdot 10^{-13}$
20	$6.545 \cdot 10^{17}$	$1.415 \cdot 10^{-11}$	$2.939 \cdot 10^{-13}$	20	$6.645 \cdot 10^{17}$	$1.183 \cdot 10^{-11}$	$8.489 \cdot 10^{-14}$

Table 7. Second order rate coefficients determined for the acetaldehyde + OH reaction at 298 K.

The following table contains the OH yields derived from the rate coefficients at the different pressures.

p/ Torr	M_{tot} / cm^{-3}	OH yield	σ(OH yield)	1/OH yield	σ(1/OH yield)
1	$3.343 \cdot 10^{16}$	0.6959	0.0405	1.4370	0.0836
1	$3.415 \cdot 10^{16}$	0.7269	0.0237	1.3758	0.0449
2.5	$7.920 \cdot 10^{16}$	0.5813	0.0191	1.7204	0.0564
3.5	$1.100 \cdot 10^{17}$	0.4682	0.0175	2.1358	0.0798
5	$1.605 \cdot 10^{17}$	0.4108	0.0144	2.4341	0.0851
10	$3.422 \cdot 10^{17}$	0.2563	0.0082	3.9010	0.1240
15	$5.024 \cdot 10^{17}$	0.1813	0.0061	5.5154	0.1861
20	$6.683 \cdot 10^{17}$	0.1305	0.0052	7.6609	0.3041
20	$6.645 \cdot 10^{17}$	0.1224	0.0039	8.1715	0.2620

Table 8. Hydroxyl radical yields calculated from the second order rate coefficients at each pressure.

Plotting the inverse of the OH yield against the total pressure, a linear relationship can be found as suggested by the simple one step relaxation model. By fitting a straight line, we obtain the ratio of quenching and decomposition rate coefficients as the slope. The Stern-Volmer plot and the linear fit can be seen in the following figure.
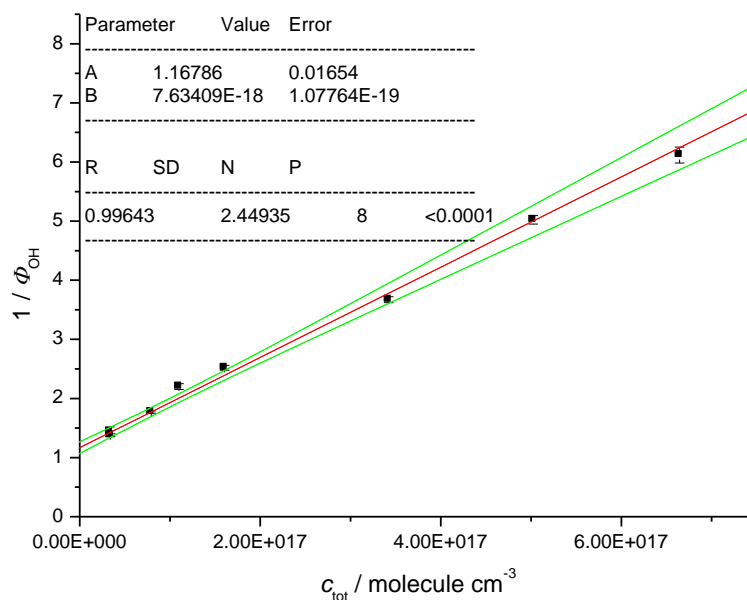

Figure 8. Stern-Volmer plot of the measured yields of the decomposition channel into OH for acetaldehyde. $T = 298$ K.

According to the fit the ratio of the rate coefficients is the following.

$$\frac{k_{quench}}{k_{decomp}} = (7.63 \pm 0.11) \cdot 10^{-18} \text{ cm}^3 \text{ molecule}^{-1}$$

The intercept of the fit is 1.17. The accuracy of the fit is sufficient for the value of 1 to lie outside the confidence intervals. This means that when extrapolating to zero pressure where no collisional relaxation can occur, the yield of the OH recycling channel is not unity. This suggests that another decomposition channel is also available which does not produce hydroxyl radicals and the yield of this channel is approximately 20% when extrapolating to zero pressure. We believe this to be a decomposition of the CH_3CO radicals into CH_3, CO due to the exothermicity of the hydrogen abstraction by OH (~120 kJ/mol).

$$[CH_3C(O)\bullet]^* \rightarrow CH_3 + CO \qquad \text{(R10)}$$

Similar observations have been made during MS-TOF measurements of acetylene yields after its reaction with hydroxyl radicals and chlorine atoms using MS-TOF technique by Neil Howes[54]. Methyl radical concentrations were monitored after the hydrogen abstraction from acetaldehyde. It was found that about 20-25% of the acetyl radicals decompose into methyl radicals after hydrogen abstraction by OH. This ratio is similar to the value that was obtained from the intercept of the Stern-Volmer plot.

Another set of experiments were performed at 212 K to characterise the temperature dependence of the reaction. This temperature was achieved using chloroform − dry ice bath.

Nitrogen				Oxygen			
p/ Torr	M_{tot} / cm^{-3}	k /cm^3 mol^{-1} s^{-1}	$\sigma(k)$	p/ Torr	M_{tot} / cm^{-3}	k / cm^3 mol^{-1} s^{-1}	$\sigma(k)$
1	$4.55\cdot10^{16}$	$2.127\cdot10^{-11}$	$2.319\cdot10^{-13}$	1	$4.744\cdot10^{16}$	$7.552\cdot10^{-12}$	$2.608\cdot10^{-13}$
2.5	$1.14\cdot10^{17}$	$2.141\cdot10^{-11}$	$6.730\cdot10^{-13}$	2.5	$1.106\cdot10^{17}$	$1.203\cdot10^{-11}$	$3.493\cdot10^{-13}$
3.5	$1.59\cdot10^{17}$	$2.111\cdot10^{-11}$	$2.532\cdot10^{-13}$	3.5	$1.530\cdot10^{17}$	$1.332\cdot10^{-11}$	$1.786\cdot10^{-13}$
5	$2.28\cdot10^{17}$	$1.970\cdot10^{-11}$	$4.810\cdot10^{-13}$	5	$2.292\cdot10^{17}$	$1.422\cdot10^{-11}$	$1.185\cdot10^{-13}$
7.5	$3.42\cdot10^{17}$	$2.047\cdot10^{-11}$	$2.986\cdot10^{-13}$	7.5	$3.352\cdot10^{17}$	$1.583\cdot10^{-11}$	$1.493\cdot10^{-13}$
9	$4.1\cdot10^{17}$	$2.047\cdot10^{-11}$	$1.749\cdot10^{-13}$	9	$3.953\cdot10^{17}$	$1.540\cdot10^{-11}$	$1.814\cdot10^{-13}$
10	$4.55\cdot10^{17}$	$2.105\cdot10^{-11}$	$1.287\cdot10^{-13}$	10	$4.670\cdot10^{17}$	$1.639\cdot10^{-11}$	$2.834\cdot10^{-13}$

Table 9. Second order rate coefficients determined for the acetaldehyde + OH reaction at 212 K.

The following table contains the OH yields for each pressure.

p/ Torr	M_{tot} / cm^{-3}	Φ_{OH}	$\sigma(\Phi_{OH})$	$1/\Phi_{OH}$	$\sigma(1/\Phi_{OH})$
1	4.744·1016	0.637	0.0369	1.5709	0.0911
2.5	1.106·1017	0.421	0.0231	2.3754	0.1304
3.5	1.530·1017	0.359	0.0174	2.7868	0.1352
5	2.292·1017	0.316	0.0149	3.1694	0.1501
7.5	3.352·1017	0.238	0.0113	4.1998	0.1998
9	3.953·1017	0.259	0.0124	3.8646	0.1858
10	4.670·1017	0.211	0.0105	4.7334	0.2353

Table 10. Hydroxyl radical yields calculated from the second order rate coefficients at each pressure.

Again we can obtain the ratio of quenching and dissociation by plotting the inverse of the OH yield against the total pressure.
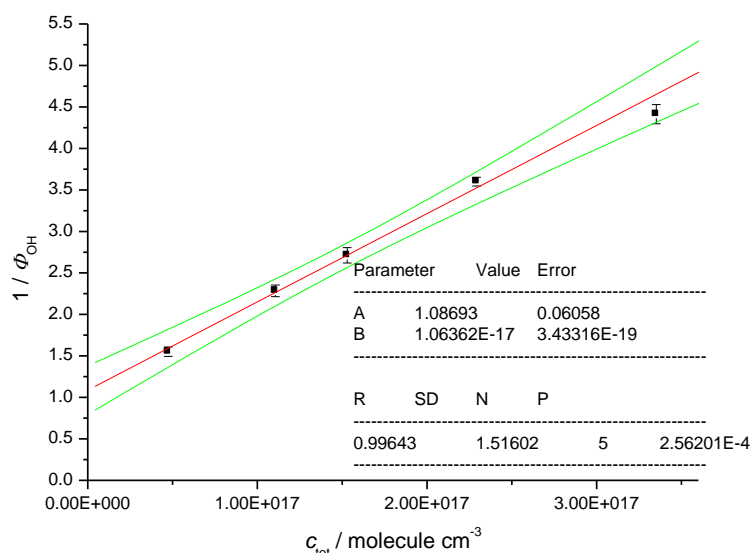

Figure 9. Stern-Volmer plot of the measured yields of the decomposition channel into OH for acetaldehyde. $T = 212$ K.

According to the fit the ratio of the rate coefficients is the following.

$$\frac{k_{quench}}{k_{decomp}} = (1.063 \pm 0.034) \cdot 10^{-17} \text{ cm}^3 \text{ molecule}^{-1}$$

The intercept of the fit is 1.08 which is lower than the value obtained at room temperature, and the value of 1 is within the confidence intervals of the fit.

Both the increased ratio between quenching and decomposition, and the decreased value of the intercept are expected at lower temperatures. As the molecules have less energy, they are less likely to pass the energy barrier involved in the hydrogen abstraction step. The secondary decomposition channel is also expected to become significant at lower temperatures, since relaxation of the CH_3CO radicals is faster at lower temperatures.

Master equation simulations of the reaction of acetyl + O_2 at the conditions of the measurements were performed. The aim was to determine if the potential energy surface previously published on this topic by Carr et al.[11] is consistent with the data I have measured. The potential energy surface was calculated using the G3X(MP2)-RAD method. The PES can be seen in the following figure.
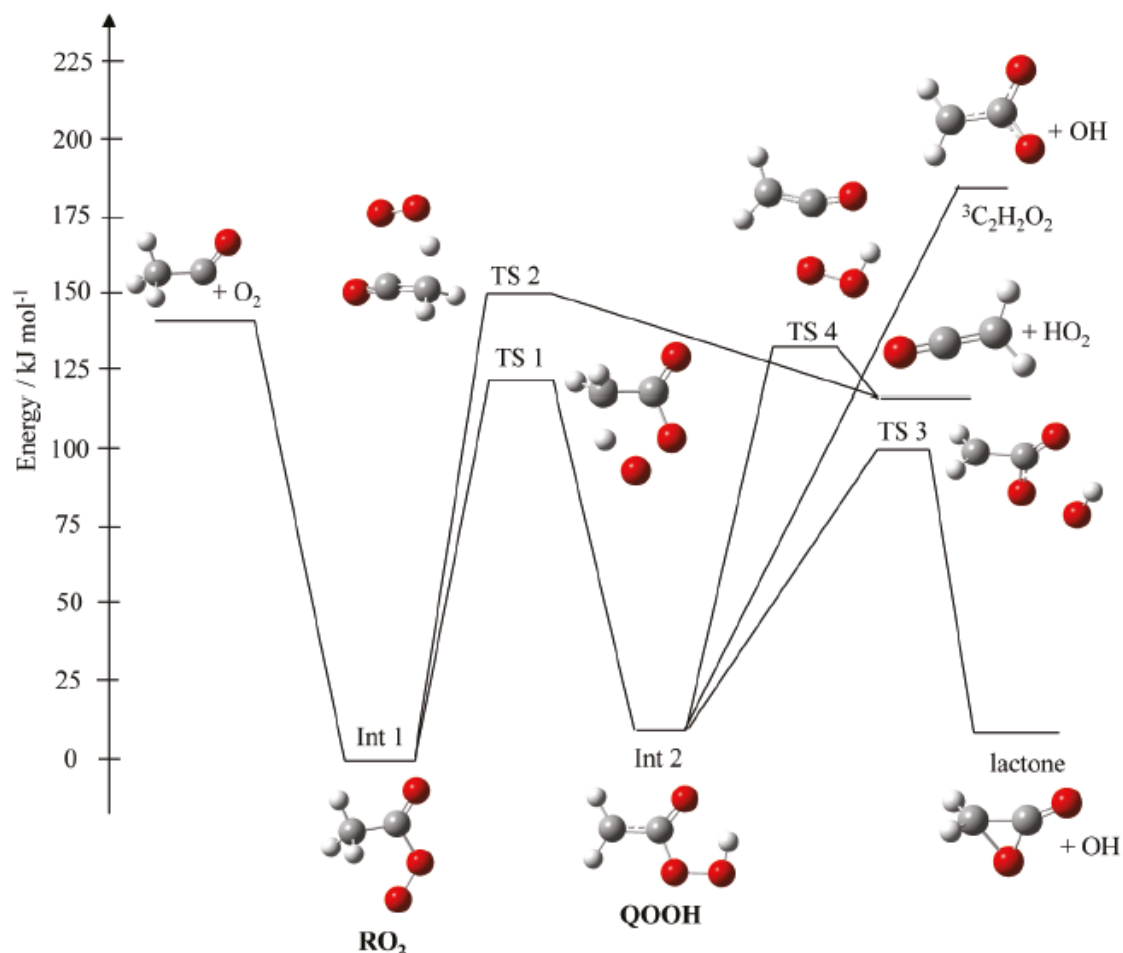

Figure 10. Potential energy surface for the acetyl + O_2 reaction. Energies are in kJ/mol, calculated using the G3X(MP2)-RAD method. Energies are relative to the peroxy radical ground state. Figure taken from paper of Carr et al.[11]

The potential energy surface contains decomposition pathways, but at room temperature only decomposition into OH and lactone or relaxation are viable channels for the peroxy radical. All other reactions were excluded from the master equation simulations.

Based on this potential energy surface the intercept of 1.17 on the Stern-Volmer plot of the room temperature data cannot be explained. There is no decomposition channel available that does not produce OH and has a sufficiently low energy barrier and it does not contain the assumed decomposition of the CH_3CO radicals into CH_3, CO.

The simplest way to address this issue is to divide all inverse yields with the value of the intercept. This way the modified data will reflect only the effect of the OH decomposition channel on the measured yields, allowing the simulation results obtained with the PES to be easily interpreted. This method requires the assumption, that the ratio of decomposition into OH and decomposition into other products is constant with pressure.

As a first step the $<\Delta E>_{down}$ parameter was fitted to the experimental data using the inbuilt fitting function of MESMER. Assuming a temperature independent energy transfer parameter, the first fit was performed to both room temperature and 212 K data. A $<\Delta E>_{down}$ parameter of 378 cm^{-1} was obtained, which can be considered a realistic value for nitrogen bath gas. The results of the simulations can be seen in the following figures.

Figure 11. Stern-Volmer plots of the measured and simulated OH yields. Simulations have been performed using the PES reported by Blitz et al., and a fitted $<\Delta E>_{down}$ parameter of 378 cm^{-1}. Black dots and blue continuous line show measured and simulated data respectively.

The results show good agreement with the measured results, with only a slight systematic under prediction at 212 K. To address this I attempted to fit the parameter independently for the data measured at the two different temperatures. I obtained $<\Delta E>_{down}$

values of 360 cm^{-1} and 394 cm^{-1} for 298 K and 212 K respectively. The results of the fits can be seen in the following figures.
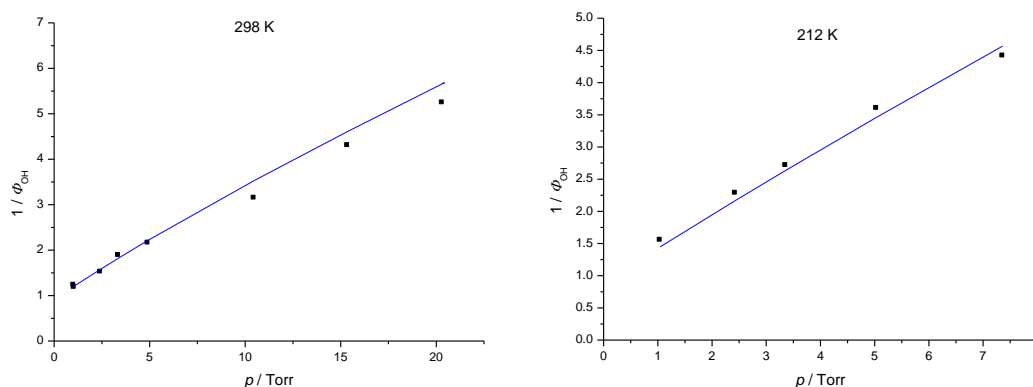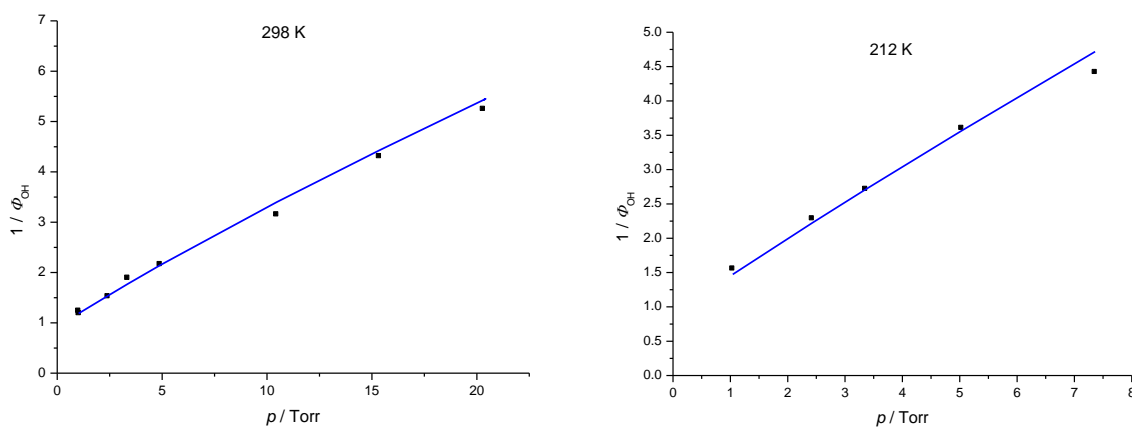

Figure 12. Stern-Volmer plots of the measured and simulated OH yields. Simulations have been performed using the PES reported by Blitz et al., and a fitted $<\Delta E>_{down}$ parameter of 360 cm^{-1} and 394 cm^{-1} respectively. Black dots and blue continuous line show measured and simulated data respectively.

It is generally expected that the $<\Delta E>_{down}$ parameter decreases with temperature and the results are in agreement with this. However as only two temperatures have been investigated in a narrow temperature range the temperature dependence of the $<\Delta E>_{down}$ parameter cannot be characterised using only these results.

Propionaldehyde

I have performed a series of experiments investigating the propionaldehyde + OH reaction, to determine the yield of the decomposition channel into OH in presence of oxygen. The experiments were conducted at room temperature and in the pressure range of 2-25 Torr. The obtained rate constants and OH yields can be seen in the following tables.

Nitrogen				Oxygen			
p/ Torr	M_{tot} / cm^{-3}	k /cm^3 mol^{-1} s^{-1}	$\sigma(k)$	p/ Torr	M_{tot} / cm^{-3}	k / cm^3 mol^{-1} s^{-1}	$\sigma(k)$
2	$6.54 \cdot 10^{16}$	$1.82 \cdot 10^{-11}$	$4.39 \cdot 10^{-13}$	2	$7.01 \cdot 10^{16}$	$3.32 \cdot 10^{-12}$	$1.90 \cdot 10^{-13}$
5	$1.63 \cdot 10^{17}$	$1.73 \cdot 10^{-11}$	$2.93 \cdot 10^{-13}$	5	$1.68 \cdot 10^{17}$	$6.95 \cdot 10^{-12}$	$2.19 \cdot 10^{-13}$
7.5	$2.45 \cdot 10^{17}$	$1.74 \cdot 10^{-11}$	$2.85 \cdot 10^{-13}$	7.5	$2.47 \cdot 1^{017}$	$9.17 \cdot 10^{-12}$	$2.37 \cdot 10^{-13}$
7.5	$2.45 \cdot 10^{17}$	$1.91 \cdot 10^{-11}$	$4.15 \cdot 10^{-13}$	7.5	$2.45 \cdot 10^{17}$	$1.05 \cdot 10^{-11}$	$2.49 \cdot 10^{-13}$
10	$3.27 \cdot 10^{17}$	$1.74 \cdot 10^{-11}$	$2.85 \cdot 10^{-13}$	10	$3.31 \cdot 10^{17}$	$1.07 \cdot 10^{-11}$	$2.16 \cdot 10^{-13}$
12.5	$4.09 \cdot 10^{17}$	$1.80 \cdot 10^{-11}$	$3.22 \cdot 10^{-13}$	12.5	$4.11 \cdot 10^{17}$	$1.29 \cdot 10^{-11}$	$1.87 \cdot 10^{-13}$
12.5	$4.09 \cdot 10^{17}$	$1.91 \cdot 10^{-11}$	$3.33 \cdot 10^{-13}$	12.5	$3.89 \cdot 10^{17}$	$1.29 \cdot 10^{-11}$	$3.88 \cdot 10^{-13}$
15	$4.90 \cdot 10^{17}$	$1.89 \cdot 10^{-11}$	$1.98 \cdot 10^{-13}$	15	$5.00 \cdot 10^{17}$	$1.32 \cdot 10^{-11}$	$2.15 \cdot 10^{-13}$
17.5	$5.72 \cdot 10^{17}$	$1.98 \cdot 10^{-11}$	$3.22 \cdot 10^{-13}$	17.5	$5.77 \cdot 10^{17}$	$1.48 \cdot 10^{-11}$	$2.36 \cdot 10^{-13}$
20	$6.54 \cdot 10^{17}$	$1.87 \cdot 10^{-11}$	$2.17 \cdot 10^{-13}$	20	$6.75 \cdot 10^{17}$	$1.50 \cdot 10^{-11}$	$3.38 \cdot 10^{-13}$
22.5	$7.36 \cdot 10^{17}$	$2.03 \cdot 10^{-11}$	$2.05 \cdot 10^{-13}$	22.5	$7.27 \cdot 10^{17}$	$1.65 \cdot 10^{-11}$	$3.04 \cdot 10^{-13}$
25	$8.18 \cdot 10^{17}$	$1.96 \cdot 10^{-11}$	$2.07 \cdot 10^{-13}$	25	$8.13 \cdot 10^{17}$	$1.63 \cdot 10^{-11}$	$5.48 \cdot 10^{-13}$
25	$8.18 \cdot 10^{17}$	$1.88 \cdot 10^{-11}$	$3.78 \cdot 10^{-13}$	25	$8.13 \cdot 10^{17}$	$1.61 \cdot 10^{-11}$	$3.44 \cdot 10^{-13}$

Table 11. Second order rate coefficients determined for the propionaldehyde + OH reaction at 298 K.

p/ Torr	M_{tot} / cm^{-3}	Φ_{OH}	$\sigma(\Phi_{OH})$	$1/\Phi_{OH}$	$\sigma(1/\Phi_{OH})$
2	0.818	0.0508	1.223	0.0760	0.818
5	0.599	0.0214	1.669	0.0597	0.599
7.5	0.473	0.0145	2.113	0.0646	0.473
7.5	0.447	0.0144	2.235	0.0718	0.447
10	0.386	0.0100	2.591	0.0675	0.386
12.5	0.286	0.0066	3.493	0.0804	0.286
12.5	0.325	0.0113	3.075	0.1066	0.325
15	0.302	0.0058	3.312	0.0641	0.302
17.5	0.249	0.0057	4.009	0.0913	0.249
20	0.201	0.0051	4.985	0.1266	0.201
22.5	0.184	0.0039	5.439	0.1140	0.184
25	0.164	0.0058	6.096	0.2141	0.164
25	0.147	0.0043	6.806	0.1997	0.147

Table 12. Hydroxyl radical yields calculated from the second order rate coefficients at each pressure.

I have plotted a Stern-Volmer diagram based on the obtained data. It was found that the relationship between the inverse of the OH yield and the total concentration could be described as linear. The Stern-Volmer plot and the fit can be seen in the following figure.
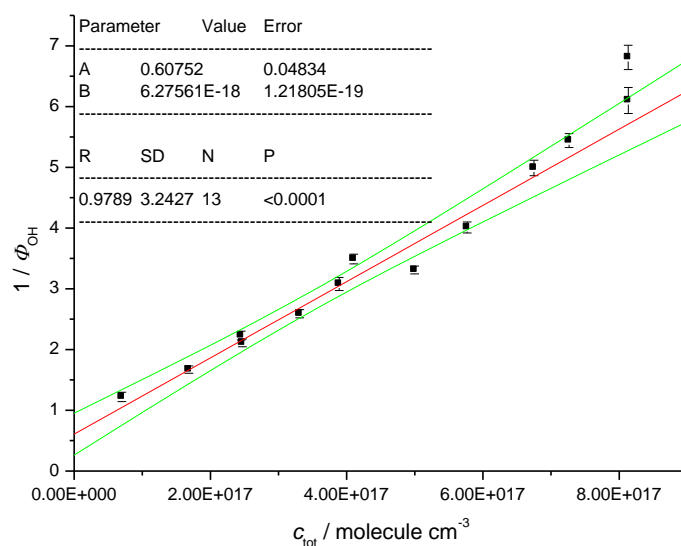

Figure 13. Stern-Volmer plot of the measured yields of the decomposition channel into OH for propionaldehyde. $T = 298$ K.

According to the fit the ratio of the rate coefficients is the following.

$$\frac{k_{quench}}{k_{decomp}} = \left(6.27 \pm 0.12\right) \cdot 10^{-18} \text{ cm}^3 \text{ molecule}^{-1}$$

The intercept of the fit is 0.6 but the 95% confidence intervals still allow for a value of 1. An intercept value that is lower than one would mean that if no relaxation occurs, more hydroxyl radicals would be produced that reacted with the aldehyde. According to our current understanding of the system this is not feasible.

Apart from experimental uncertainty, a possible explanation would be that the relationship between the inverse OH yield and pressure is slightly curved. Such curvature would appear if not only the $R(O)O_2$ radicals could relax due to collisions and the one-step relaxation model would be no longer valid.

Liming Wang has calculated the potential energy surface describing the possible reactions of the propionyl radical with oxygen using ROCBS-QB3 level of theory[55]. The potential energy surface can be seen in the following figure, as plotted by MESMER.
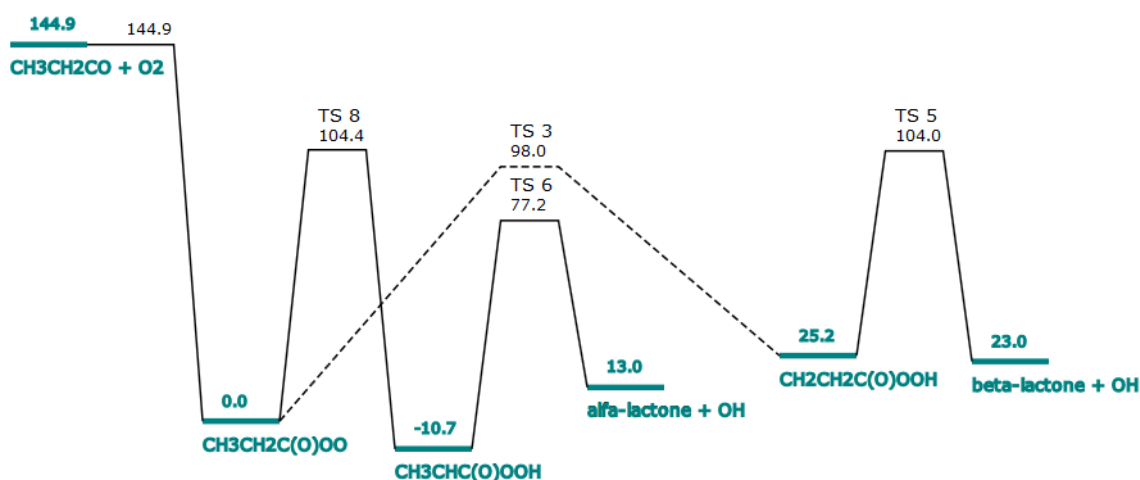
Figure 14. Potential energy surface for the propionyl + O_2 reaction. Energies are in kJ/mol.

It was found, that the β-Q(O)OOH radical is significantly more stable (-11 kJ/mol compared to the respective $R(O)O_2$ radical) compared to the Q(O)OOH radical in the acetyl + O_2 system (+12 kJ/mol compared to the respective $R(O)O_2$ radical).

Currently no master equation simulations of the system have been performed but it is expected that these simulations will help understand the exact mechanism of this reaction. Further measurements at higher and very low pressures will also have to be performed to confirm or refute the non-linear relationship between the inverse OH yields and pressure.

Butyraldehyde

I have performed a series of experiments investigating the butyraldehyde + OH reaction, to determine the yield of the decomposition channel into OH in presence of oxygen. The experiments were conducted at room temperature (298 K) and in the pressure range of 2.5-20 Torr.

The obtained rate constants and OH yields can be seen in the following tables.

Nitrogen				Oxygen			
p/ Torr	M_{tot} / cm^{-3}	k /cm^3 mol^{-1} s^{-1}	$\sigma(k)$	p/ Torr	M_{tot} / cm^{-3}	k /cm^3 mol^{-1} s^{-1}	$\sigma(k)$
2.5	$8.181 \cdot 10^{16}$	$2.366 \cdot 10^{-11}$	$4.920 \cdot 10^{-13}$	2.5	$8.329 \cdot 10^{16}$	$6.018 \cdot 10^{-12}$	$4.013 \cdot 10^{-13}$
5	$1.636 \cdot 10^{17}$	$2.308 \cdot 10^{-11}$	$2.096 \cdot 10^{-13}$	5	$1.644 \cdot 10^{17}$	$1.084 \cdot 10^{-11}$	$3.526 \cdot 10^{-13}$
7.5	$2.454 \cdot 10^{17}$	$2.269 \cdot 10^{-11}$	$3.357 \cdot 10^{-13}$	7.5	$2.433 \cdot 10^{17}$	$1.283 \cdot 10^{-11}$	$1.656 \cdot 10^{-13}$
10	$3.272 \cdot 10^{17}$	$2.369 \cdot 10^{-11}$	$1.870 \cdot 10^{-13}$	10	$3.296 \cdot 10^{17}$	$1.543 \cdot 10^{-11}$	$2.991 \cdot 10^{-13}$
13	$4.254 \cdot 10^{17}$	$2.316 \cdot 10^{-11}$	$2.253 \cdot 10^{-13}$	13	$4.381 \cdot 10^{17}$	$1.637 \cdot 10^{-11}$	$1.524 \cdot 10^{-13}$
17	$5.563 \cdot 10^{17}$	$2.312 \cdot 10^{-11}$	$1.456 \cdot 10^{-13}$	17	$5.628 \cdot 10^{17}$	$1.789 \cdot 10^{-11}$	$2.763 \cdot 10^{-13}$
20	$6.545 \cdot 10^{17}$	$2.430 \cdot 10^{-11}$	$3.245 \cdot 10^{-13}$	20	$6.530 \cdot 10^{17}$	$1.978 \cdot 10^{-11}$	$2.971 \cdot 10^{-13}$

Table 13. Second order rate coefficients determined for the butyraldehyde + OH reaction at 298 K.

p/ Torr	M_{tot} / cm^{-3}	Φ_{OH}	$\sigma(\Phi_{OH})$	$1/ \Phi_{OH}$	$\sigma(\Phi_{OH})$
2.5	$8.329 \cdot 10^{16}$	0.746	0.0521	1.341	0.094
5	$1.644 \cdot 10^{17}$	0.530	0.0179	1.886	0.064
7.5	$2.433 \cdot 10^{17}$	0.434	0.0085	2.302	0.045
10	$3.296 \cdot 10^{17}$	0.349	0.0073	2.869	0.060
13	$4.381 \cdot 10^{17}$	0.293	0.0039	3.410	0.046
17	$5.628 \cdot 10^{17}$	0.226	0.0038	4.416	0.074
20	$6.530 \cdot 10^{17}$	0.186	0.0037	5.385	0.108

Table 14. Hydroxyl radical yields calculated from the second order rate coefficients at each pressure.

I found that the relation between the inverse of the OH yield and total pressure can be described linearly at these experimental conditions. This suggests that the collisional relaxation is only significant for the peroxy radical form of the molecule.
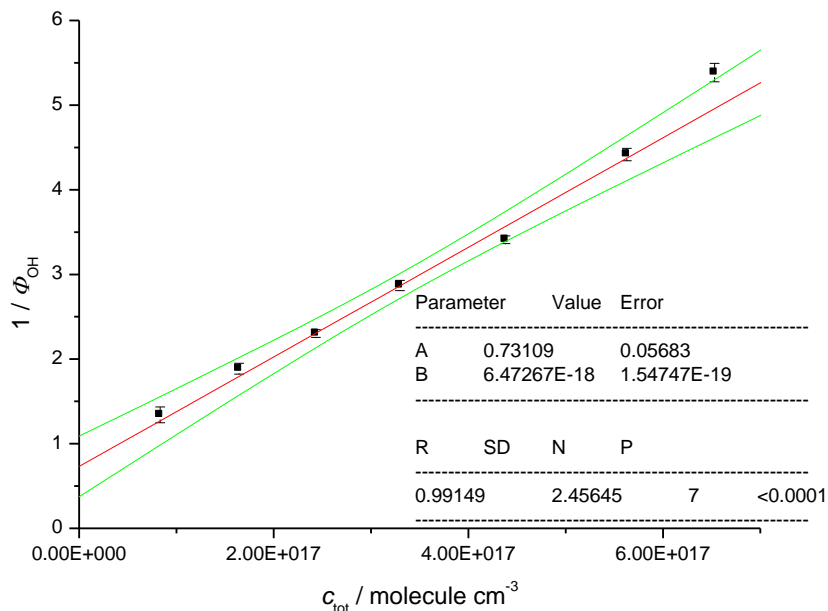

Figure 15. Stern-Volmer plot of the measured yields of the decomposition channel into OH for butyraldehyde. $T = 298$ K.

According to the fit the ratio of the rate coefficients is the following.

$$\frac{k_{quench}}{k_{decomp}} = (6.47 \pm 0.15) \cdot 10^{-18} \text{ cm}^3 \text{ molecule}^{-1}$$

The confidence intervals of the fit include the intercept value of 1, however similarly to the results obtained for propionaldehyde the mean value of the intercept is below one. This could suggest that the stable Q(O)OOH radicals are forming due to collisional relaxation. Further measurements at higher and very low pressures are needed in this case too to confirm this possibility.

Methacrolein

The rate constant of the reaction between methacrolein and OH has been measured to determine if there is a significant amount of OH recycling occurring in the presence of O_2, as suggested by da Silva[6]. Experiments at 5, 2.5 and 1 Torr pressures and at room temperature have been performed. For the experiments conducted in the presence of oxygen, approximately 20% oxygen was added to the bath gas in the reaction cell.

The results can be seen in the following table.

Nitrogen				Oxygen			
p/ Torr	M_{tot} / cm^{-3}	k /cm^3 mol^{-1} s^{-1}	$\sigma(k)$	p/ Torr	M_{tot} / cm^{-3}	k /cm^3 mol^{-1} s^{-1}	$\sigma(k)$
5	$1.64 \cdot 10^{17}$	$2.031 \cdot 10^{-11}$	$2.429 \cdot 10^{-13}$	5	$1.745 \cdot 10^{17}$	$2.19 \cdot 10^{-11}$	$1.44 \cdot 10^{-13}$
2.5	$8.18 \cdot 10^{16}$	$1.942 \cdot 10^{-11}$	$1.941 \cdot 10^{-13}$	2.5	$7.922 \cdot 10^{16}$	$2.51 \cdot 10^{-11}$	$2.06 \cdot 10^{-12}$
				2.5	$8.23 \cdot 10^{16}$	$2.67 \cdot 10^{-11}$	$1.44 \cdot 10^{-12}$
1	$3.27 \cdot 10^{16}$	$2.101 \cdot 10^{-11}$	$6.641 \cdot 10^{-13}$	1	$3.245 \cdot 10^{16}$	$2.58 \cdot 10^{-11}$	$6.67 \cdot 10^{-13}$

Table 15. Second order rate coefficients determined for the methacrolein + OH reaction at 298 K.

The first batch of experiments showed an increase in the rate coefficient in the presence of oxygen. This was considered to be due to an experimental error, since there is no theoretically feasible way for this effect.

The paper of da Silva suggested that OH recycling would occur via alkylperoxy radicals which retain most of their excess energy from the OH addition when it is formed by association with oxygen. He called this state doubly excited, where the molecule has excess energy both from the OH and subsequent oxygen addition. The potential energy surface calculated by da Silva for the hydroxyl radical and oxygen addition can be seen in the following figure.
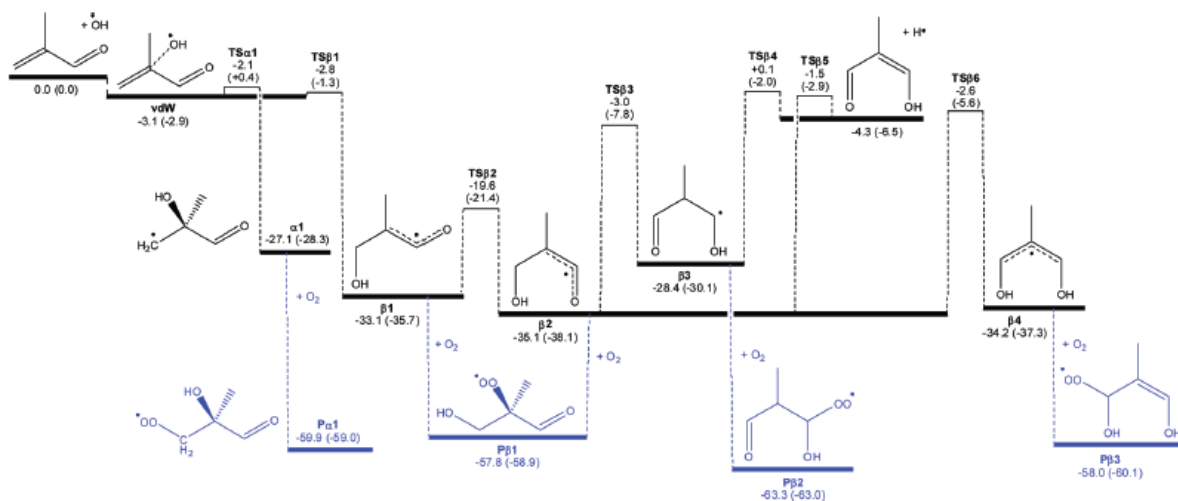
Figure 16. Potential energy surface for the reaction of methacrolein with hydroxyl radicals and oxygen. Values were calculated using G3SX (M06-2X/aug-cc-pVTZ) method, and are given in kcal mol^{-1}. Figure taken from paper of da Silva[6].

It was predicted by da Silva that the main products of the OH and following O_2 addition would be the Pβ1 and Pβ2 isomers which could have approximately 40 kcal mol^{-1} excess energy if doubly activated.

This would mean that the yield of OH recycling could decrease if the molecules lose some of their initial excess energy via collisions before reacting with oxygen. The experiments were repeated using only oxygen as the bath gas in the experiment. This way the rate of reaction with oxygen would be maximized, also maximizing the amount of doubly excited alkylperoxy radicals. The disadvantage of using oxygen is that is quenches the fluorescence of OH approximately more efficiently than nitrogen, causing worse signal to noise ratio in the measurements.

The next set of results showed no change within error, when changing the bath gas from nitrogen to oxygen. Since the results were the same within experimental error, it can be said that no OH recycling takes place at these conditions. The results can be seen in the following table.

43

Nitrogen				Oxygen			
p/ Torr	M_{tot} / cm^{-3}	k /cm^3 mol^{-1} s^{-1}	$\sigma(k)$	p/ Torr	M_{tot} / cm^{-3}	k /cm^3 mol^{-1} s^{-1}	$\sigma(k)$
1	$3.27 \cdot 10^{-16}$	$2.053 \cdot 10^{-11}$	$2.826 \cdot 10^{-13}$	5	$1.625 \cdot 10^{17}$	$2.20 \cdot 10^{-11}$	$2.83 \cdot 10^{-13}$
				2.5	$8.07 \cdot 10^{16}$	$2.231 \cdot 10^{-11}$	$2.789 \cdot 10^{-13}$
				1	$3.245 \cdot 10^{16}$	$2.02 \cdot 10^{-11}$	$4.95 \cdot 10^{-13}$

Table 16. Second order rate coefficients determined for the methacrolein + OH reaction at 298 K.

The most probable reason for the lack of hydroxyl radical recycling is that it would require double activation. If the association reaction with oxygen is relatively slow, it is possible for the radicals obtained from the OH addition to lose all their excess energy before further reaction. This would prevent any unimolecular decomposition into hydroxyl radicals.

In comparison with previous studies, the rate constant that was obtained in nitrogen bath gas is significantly lower. The uncertainty in the determination of the rate constant arises primarily from the uncertainty of the concentration of methacrolein in the sample bulb. It was found difficult to fill the sample bulb with methacrolein due to its low vapour pressure and its strong adsorption to the walls of the vacuum line, which made the determination of absolute bimolecular rate constants uncertain.

Acrolein

The rate constant of the reaction between acrolein and OH has been measured to determine if there is a significant amount of OH recycling possible in the presence of O_2. First experiments were performed at 5 Torr pressure, at room temperature. For the experiments in oxygen approximately 20% oxygen was used in the bath gas and nitrogen as the remaining amount. No evidence for OH recycling based on these experiments was found.

Similarly to methacrolein, Asatryan et al.[7] suggests that OH recycling is expected to occur via doubly excited peroxy radicals. I repeated the experiment using only oxygen as a diluting gas at 2 and 5 Torr pressures. In each experiment no decrease in the rate coefficient could be seen, therefore no significant OH recycling occurs at these conditions.

It was considered possible that the reason for not observing any OH recycling is that due to its excess energy the radical formed by hydrogen abstraction undergoes decomposition before it can react with oxygen. Further experiments were performed at 50 Torr and 20% oxygen ratio of the bath gas. At such a relatively high pressure the radical obtained from the OH addition quickly loses its excess energy and forms a peroxy radical with oxygen in its relaxed state. Based on the results, no OH recycling was observed in this case either.

The results can be seen in the following table.

Nitrogen				Oxygen				
p/ Torr	M_{tot} / cm^{-3}	k /cm^3 mol^{-1} s^{-1}	$\sigma(k)$	p/ Torr	O_2 fraction	M_{tot} / cm^{-3}	k / cm^3 mol^{-1} s^{-1}	$\sigma(k)$
5	$1.636 \cdot 10^{17}$	$1.454 \cdot 10^{-11}$	$4.896 \cdot 10^{-13}$	5	20%	$1.734 \cdot 10^{17}$	$1.50 \cdot 10^{-11}$	$6.22 \cdot 10^{-13}$
				5	100%	$1.680 \cdot 10^{17}$	$1.54 \cdot 10^{-11}$	$3.94 \cdot 10^{-13}$
2	$6.545 \cdot 10^{16}$	$1.512 \cdot 10^{-11}$	$1.143 \cdot 10^{-13}$	2	100%	$7.430 \cdot 10^{16}$	$1.55 \cdot 10^{-11}$	$5.96 \cdot 10^{-13}$
50	$1.636 \cdot 10^{18}$	$1.563 \cdot 10^{-11}$	$4.338 \cdot 10^{-13}$	50	10%	$1.694 \cdot 10^{18}$	$1.59 \cdot 10^{-11}$	$6.25 \cdot 10^{-13}$

Table 17. Second order rate coefficients determined for the acrolein + OH reaction at 298 K.

The results suggest that OH recycling does not occur either at low pressures, where the formation of the peroxy radical can often form in a doubly excited state. It doesn't occur at higher pressure either where the excitation energy gained from the reaction with OH is lost via collisions.

The reason for lack of hydroxyl radical recycling is assumed to be similar as in the case of methacrolein. The relative rates of relaxation after OH addition and the oxygen

addition step probably hinder the formation of doubly activated radicals, which prevents unimolecular decomposition.

The rate constant for the reaction of acrolein with hydroxyl radicals was found to be lower than previously reported values in the literature. Similar difficulties as in the case of methacrolein were encountered while preparing the sample bulbs which could explain this discrepancy.

Summary

I have investigated the hydroxyl radical recycling occurring during the reaction of OH with acetaldehyde, propionaldehyde, and butyraldehyde. The pressure dependence of the hydroxyl radical recycling was quantified in the pressure range of approximately 2 – 20 Torr at room temperature. The hydroxyl radical recycling during the acetaldehyde + OH reaction was also measured at 212 K.

In each case the relationship between the pressure and hydroxyl radical yields could be described by a simple one-step relaxation model and the ratio of the rate of collisional quenching and unimolecular decomposition was determined.

In the case of acetaldehyde it was found that a decomposition channel that does not produce OH also exists, with a yield of 15-20%. This is assumed to be the decomposition of acetyl radicals into CH_3 and CO after the abstraction of a hydrogen atom from acetaldehyde by OH. This assumption is supported by MS-TOF measurements performed by Neil Howes[54], who observed that acetyl radicals produced by the acetaldehyde + OH reaction decompose into methyl radicals with a yield of 20-25%.

Master equation simulations of the acetyl + O2 reaction were also performed. It was found that the experimental results are consistent with the potential energy surface published by Carr et al[11].

Propionaldehyde and butyraldehyde were found to behave similarly. Both exhibited nearly identical ratios of relaxation and decomposition rates. No decomposition channel has significant yield other than decomposition into OH at conditions of the experiments. The relation between the inverse OH yields and pressure suggest a slight non-linearity. This could be interpreted by collisional relaxation of both $R(O)O_2$ and $Q(O)OOH$ radicals, but further and more accurate measurements would be required to confirm this effect.

Acrolein and methacrolein were also investigated to determine if a similar recycling of hydroxyl radicals can take place. In both cases the experiments yielded a negative results even at low pressures, excluding the possibility these molecules contribution to OH recycling at atmospheric conditions.

Összefoglalás

Munkám során aldehidek hidroxil-gyök visszanyerési reakcióit vizsgáltam oxigén jelenlétében. Megállapítottam a hidroxil-gyök visszanyerési hozamát acetaldehidnek, propionaldehidnek és butiraldehidnek 2-20 Torr nyomástartományban szobahőmérsékleten. Acetaldehid esetén 212 K hőméréségletet is végeztem kísérleteket.

Minden esetben értelmezhető volt a hidroxil-gyök hozam nyomásfüggése egyszerű egy lépéses deaktivációs modellel. A modell alapján meghatároztam mindhárom vegyület esetén a belőlük származó alkil-peroxi-gyök ütközéses deaktivációját és az hidroxil-gyökké bomlását leíró sebességi együtthatók arányát.

Acetaldehid esetén megállapítottam egy további bomlási reakció létezését amely nem termel hidroxil-gyököket. Méréseim alapján ennek a reakciónak a hozama 15-20%. Az általam megállapított bomlási arány összhangban van a kutatócsoportunk más független eredményeivel. Niel Howes MS-TOF kísérletek alapján igazolta, hogy az acetaldehid + OH reakcióban keletkező acetil-gyök 20-25%-ban metil-gyökké és szén monoxiddá bomlik[54].

Az acetil-gyök + O_2 reakciónak elvégeztem a master equation (vezéregyenlet) alapú szimulációját. Carr és munkatárai [11] által publikált potenciális energia felületet használtam fel a számításokhoz. A szimulációk eredménye összhangban van a kísérleti eredményeimmel.

A propionaldehid és butiraldehid esetén egymáshoz hasonló eredményeket kaptam. Közel azonos nyomásfüggését tapasztalatam a hidroxil-gyök visszanyerési reakció hozamának. Egyik esetben sem tapasztaltam más bomlási reakciónak számottevő befolyását a rendszerre. A hidroxil-gyök visszanyerési reakciók hozama kis mértékű eltérést mutatott az egylépeses deaktivációs modelltől a legalacsonyabb és legmagasabb nyomásokon. Ez magyarázható lehet azzal, hogy az $R(O)O_2$ típusú gyökök ütközéses deaktivációja mellett végbemegy a $Q(O)OOH$ típusú gyökök relaxációja. További pontos kísérletek szükségesek magasabb és nagyon alacsony nyomáson az effektus igazolásához.

Hasonló kísérleteket végeztem akroleinnel és metil-akroleinnel. Célom volt megállapítani, hogy ezekben a vegyületekben is végbe tud-e menni egy hidroxil-gyök visszanyerési reakció. Mindkét esetben ki tudtam zárni, hogy számottevő hozammal visszanyerhetőek hidroxil-gyökök ezeknek a vegyületeknek esetén.

References

1. Stone, D.; Whalley, L. K.; Heard, D. E. *Chemical Society Reviews*, 41 (19), 6348-6404.(2012)

2. Tan, D.; Faloona, I.; Simpas, J. B.; Brune, W.; Shepson, P. B.; Couch, T. L.; Sumner, A. L.; Carroll, M. A.; Thornberry, T.; Apel, E.; Riemer, D.; Stockwell, W. *Journal of Geophysical Research-Atmospheres*, 106 (D20), 24407-24427.(2001)

3. Carslaw, N.; Creasey, D. J.; Harrison, D.; Heard, D. E.; Hunter, M. C.; Jacobs, P. J.; Jenkin, M. E.; Lee, J. D.; Lewis, A. C.; Pilling, M. J.; Saunders, S. M.; Seakins, P. W. *Atmospheric Environment*, 35 (27), 4725-4737.(2001)

4. Kuhn, U.; Andreae, M. O.; Ammann, C.; Araujo, A. C.; Brancaleoni, E.; Ciccioli, P.; Dindorf, T.; Frattoni, M.; Gatti, L. V.; Ganzeveld, L.; Kruijt, B.; Lelieveld, J.; Lloyd, J.; Meixner, F. X.; Nobre, A. D.; Poeschl, U.; Spirig, C.; Stefani, P.; Thielmann, A.; Valentini, R.; Kesselmeier, J. *Atmospheric Chemistry and Physics*, 7 (11), 2855-2879.(2007)

5. Da Silva, G.; Graham, C.; Wang, Z.-F. *Environmental Science & Technology*, 44 (1), 250-256.(2010)

6. da Silva, G. *Journal of Physical Chemistry A*, 116 (22), 5317-5324.(2012)

7. Asatryan, R.; da Silva, G.; Bozzelli, J. W. *Journal of Physical Chemistry A*, 114 (32), 8302-8311.(2010)

8. Michael, J. V.; Keil, D. G.; Klemm, R. B. *Journal of Chemical Physics*, 83 (4), 1630-1636.(1985)

9. Taatjes, C. A. *Journal of Physical Chemistry A*, 110 (13), 4299-4312.(2006)

10. Rosado-Reyes, C. M.; Francisco, J. S.; Szente, J. J.; Maricq, M. M.; Ostergaard, L. F. *Journal of Physical Chemistry A*, 109 (48), 10940-10953.(2005)

11. Carr, S. A.; Glowacki, D. R.; Liang, C. H.; Baeza-Romero, M. T.; Blitz, M. A.; Pilling, M. J.; Seakins, P. W. *Journal of Physical Chemistry A*, 115 (6), 1069-1085.(2011)

12. Zhu, L.; Talukdar, R. K.; Burkholder, J. B.; Ravishanker, A. R. *International Journal of Chemical Kinetics*, 40 (10), 635-646.(2008)

13. Taylor, P. H.; Yamada, T.; Marshall, P. *International Journal of Chemical Kinetics*, 38 (8), 489-495.(2006)

14. Wang, J. J.; Chen, H. B.; Glass, G. P.; Curl, R. F. *Journal of Physical Chemistry A*, 107 (49), 10834-10844.(2003)

15. Sivakumaran, V.; Crowley, J. N. *Physical Chemistry Chemical Physics*, 5 (1), 106-111.(2003)

16.	D'Anna, B.; Andresen, W.; Gefen, Z.; Nielsen, C. J. *Physical Chemistry Chemical Physics*, 3 (15), 3057-3063.(2001)

17.	Scollard, D. J.; Treacy, J. J.; Sidebottom, H. W.; Balestragarcia, C.; Laverdet, G.; Lebras, G.; Macleod, H.; Teton, S. *Journal of Physical Chemistry*, 97 (18), 4683-4688.(1993)

18.	Balestragarcia, C.; Lebras, G.; Macleod, H. *Journal of Physical Chemistry*, 96 (8), 3312-3316.(1992)

19.	Dobe, S.; Khachatryan, L. A.; Berces, T. *Berichte Der Bunsen-Gesellschaft-Physical Chemistry Chemical Physics*, 93 (8), 847-852.(1989)

20.	Semmes, D. H.; Ravishankara, A. R.; Gumpperkins, C. A.; Wine, P. H. *International Journal of Chemical Kinetics*, 17 (3), 303-313.(1985)

21.	Niki, H.; Maker, P. D.; Savage, C. M.; Breitenbach, L. P. *Journal of Physical Chemistry*, 82 (2), 132-134.(1978)

22.	Atkinson, R.; Pitts, J. N. *Journal of Chemical Physics*, 68 (8), 3581-3584.(1978)

23.	Morris, E. D.; Stedman, D. H.; Niki, H. *Journal of the American Chemical Society*, 93 (15), 3570-&.(1971)

24.	Baulch, D. L.; Cobos, C. J.; Cox, R. A.; Esser, C.; Frank, P.; Just, T.; Kerr, J. A.; Pilling, M. J.; Troe, J.; Walker, R. W.; Warnatz, J. *Journal of Physical and Chemical Reference Data*, 21 (3), 411-734.(1992)

25.	Kovacs, G.; Zador, J.; Farkas, E.; Nadasdi, R.; Szilagyi, I.; Dobe, S.; Berces, T.; Marta, F.; Lendvay, G. *Physical Chemistry Chemical Physics*, 9 (31), 4142-4154.(2007)

26.	Tyndall, G. S.; Orlando, J. J.; Kegley-Owen, C. S.; Wallington, T. J.; Hurley, M. D. *International Journal of Chemical Kinetics*, 31 (11), 776-784.(1999)

27.	Tyndall, G. S.; Orlando, J. J.; Wallington, T. J.; Hurley, M. D. *International Journal of Chemical Kinetics*, 29 (9), 655-663.(1997)

28.	Sehested, J.; Christensen, L. K.; Nielsen, O. J.; Wallington, T. J. *International Journal of Chemical Kinetics*, 30 (12), 913-921.(1998)

29.	McDade, C. E.; Lenhardt, T. M.; Bayes, K. D. *Journal of Photochemistry*, 20 (1), 1-7.(1982)

30.	Romero, M. T. B.; Blitz, M. A.; Heard, D. E.; Pilling, M. J.; Price, B.; Seakins, P. W. *Chemical Physics Letters*, 408 (4-6), 232-236.(2005)

31.	Blitz, M. A.; Heard, D. E.; Pilling, M. J. *Chemical Physics Letters*, 365 (5-6), 374-379.(2002)

32.	Carr, S. A.; Baeza-Romero, M. T.; Blitz, M. A.; Pilling, M. J.; Heard, D. E.; Seakins, P. W. *Chemical Physics Letters*, 445 (4-6), 108-112.(2007)

33.	Chen, S. Y.; Lee, Y. P. *Journal of Chemical Physics*, 132 (11), 114303.(2010)

34.	Romero, M. T. B.; Blitz, M. A.; Heard, D. E.; Pilling, M. J.; Price, B.; Seakins, P. W.; Wang, L. M. *Faraday Discussions*, 130 73-88.(2005)

35.   Devolder, P.; Dusanter, S.; Lemoine, B.; Fittschen, C. *Chemical Physics Letters*, 417 (1-3), 154-158.(2006)
36.   Le Crane, J. P.; Villenave, E.; Hurley, M. D.; Wallington, T. J.; Ball, J. C. *Journal of Physical Chemistry A*, 109 (51), 11837-11850.(2005)
37.   Baker, J.; Arey, J.; Atkinson, R. *Journal of Physical Chemistry A*, 108 (34), 7032-7037.(2004)
38.   Thevenet, R.; Mellouki, A.; Le Bras, G. *International Journal of Chemical Kinetics*, 32 (11), 676-685.(2000)
39.   Papagni, C.; Arey, J.; Atkinson, R. *International Journal of Chemical Kinetics*, 32 (2), 79-84.(2000)
40.   Kerr, J. A.; Sheppard, D. W. *Environmental Science & Technology*, 15 (8), 960-963.(1981)
41.   Audley, G. J.; Baulch, D. L.; Campbell, I. M. *Journal of the Chemical Society-Faraday Transactions I*, 77 2541-2549.(1981)
42.   Zugner, G. L.; Szilagyi, I.; Zador, J.; Szabo, E.; Dobe, S.; Song, X.; Wang, B. *Chemical Physics Letters*, 495 (4-6), 179-181.(2010)
43.   Clapp, L. J.; Jenkin, M. E. *Atmospheric Environment*, 35 (36), 6391-6405.(2001)
44.   http://www.cas.manchester.ac.uk/resactivities/atmosphericchemistry/topics/peroxyradical/, Accessed at May 14,2013
45.   Orlando, J. J.; Tyndall, G. S. *Journal of Physical Chemistry A*, 106 (51), 12252-12259.(2002)
46.   Magneron, I.; Thevenet, R.; Mellouki, A.; Le Bras, G.; Moortgat, G. K.; Wirtz, K. *Journal of Physical Chemistry A*, 106 (11), 2526-2537.(2002)
47.   Edney, E. O.; Kleindienst, T. E.; Corse, E. W. *International Journal of Chemical Kinetics*, 18 (12), 1355-1371.(1986)
48.   Atkinson, R.; Aschmann, S. M.; Pitts, J. N. *International Journal of Chemical Kinetics*, 15 (1), 75-81.(1983)
49.   Chuong, B.; Stevens, P. *International Journal of Chemical Kinetics*, 36 (1), 12-25.(2004)
50.   Chuong, B.; Stevens, P. S. *Journal of Physical Chemistry A*, 107 (13), 2185-2191.(2003)
51.   Gierczak, T.; Burkholder, J. B.; Talukdar, R. K.; Mellouki, A.; Barone, S. B.; Ravishankara, A. R. *Journal of Photochemistry and Photobiology a-Chemistry*, 110 (1), 1-10.(1997)
52.   Kleindienst, T. E.; Harris, G. W.; Pitts, J. N. *Environmental Science & Technology*, 16 (12), 844-846.(1982)
53.   Glowacki, D. R.; Liang, C.-H.; Morley, C.; Pilling, M. J.; Robertson, S. H. *Journal of Physical Chemistry A*, 116 (38), 9545-9560.(2012)
54.   Howes, N., Personal communication, 2013.
55.   Wang, L., Personal communication, 2013.